

Double diffusive instability in a tall thin slot

By NEIL J. BALMFORTH¹ AND JOSEPH A. BIELLO²

¹ Institute for Geophysics and Planetary Physics, University of California at San Diego,
La Jolla, CA 92093, USA

² Department of Astronomy and Astrophysics, University of Chicago, Chicago, IL, 60637, USA

(Received 26 August 1997 and in revised form 30 June 1998)

The linear stability of doubly diffusive convection is considered for a two-dimensional, Boussinesq fluid in a tall thin slot. For a variety of boundary conditions on the slot walls, instability sets in through zero wavenumber over a wide range of physical conditions. Long-wave equations governing the nonlinear development of the instability are derived. The form of the long-wave equations sensitively depends on the thermal and salt boundary conditions; the possible long-wave theories are catalogued. Finite-amplitude solutions and their stability are studied. In some cases the finite-amplitude solutions are not the only possible attractors and numerical solutions presenting the alternatives are given. These reveal temporally complicated dynamics.

1. Introduction

Convection in a doubly diffusing fluid is an important physical problem in a variety of contexts. Its implications have wide application in geophysics, astrophysics and industrial processes. In the standard idealization of the problem, one considers a fluid containing two diffusing components. One component is unstably stratified and drives convective motion, the other component is stably stratified and attempts to anchor the fluid against such convection. When the diffusivities are not equal, double-diffusive instability may occur; this is a central theme of this study.

We consider, in particular, the case in which the unstably stratified component diffuses quicker than the stably stratified component (normally referred to as ‘heat’ and ‘salt’ respectively, even if the constituents are different). In this circumstance, overstable oscillations set in at the onset of instability. This is customarily called the ‘diffusive’ problem, as opposed to that of the ‘salt fingers’. The novelty of the problem we consider is its geometry: two-dimensional, thermohaline convection in a tall, thin slot (figure 1).

The key feature of the slot containing the fluid is that it is thin, but not so thin that the Hele-Shaw limit is approached. That is, it is midway between the usual thermohaline configuration (Veronis 1968) and what is often referred to as Lapwood convection (Lapwood 1948). The purely thermal (singly diffusing) problem was considered earlier by Normand (1984) and Linz (1990), and is related to studies on tilted slots by Cessi & Young (1992). These authors were concerned with physical situations such as convection in rock fractures. Such geological applications are also relevant here: crystallization in a cooling magma can lead to double-diffusive effects (Chen & Turner 1980), and a vertical rock fracture containing the magma provides a natural setting of the geometry.

Other applications include industrial processes and lab experiments, where the geometry is intentionally designed (Turner 1985). Along more exotic lines, the role of

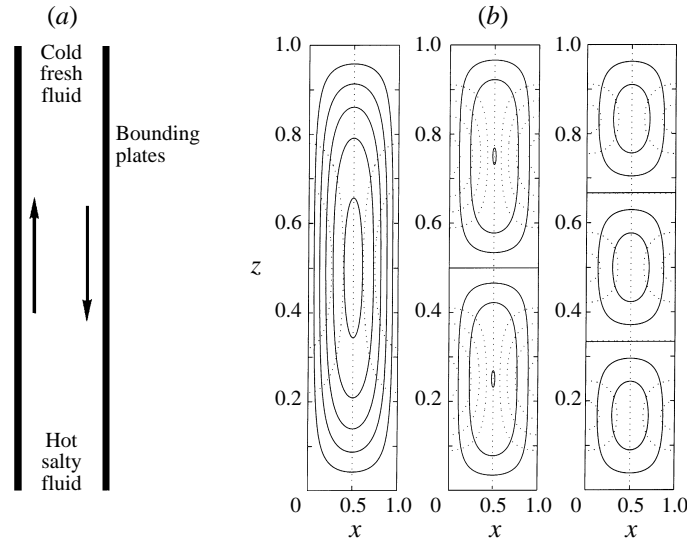


FIGURE 1. The geometry of the doubly-diffusive system, and three possible patterns of oscillatory convection in a tall, thin slot. The background profile is one of no velocity while temperature and salt have constant, negative vertical gradients (and no horizontal variation). In the first sketch we omit the upper and lower boundary conditions to make the point that the mathematical development of the problem will initially ignore these boundaries; their consideration comes later, once we have amplitude equations in terms of a long vertical coordinate. The solid lines in the three right figures indicate stream function while dashed lines are isotherms with the background gradient subtracted. The diagrams are schematic of the geometry we are considering, though for the problem we discuss, the ratio of vertical to horizontal extent is actually much greater.

buoyancy can in some situations be played by magnetic pressure and momentum. Furthermore, convection can be confined to tall thin cells by external forces such as magnetic fields and rotation; these suggest applications in astrophysics and plasma physics.

This particular study was originally motivated by a specific fluid experiment (Biello 1996) in which the apparatus took the form of a tall, thin slot. In turn, that experiment was motivated by the question of the robustness of layers in doubly diffusive convection. Experiments by Huppert & Linden (1979) show the formation of layers when water containing a stably stratified salt gradient is impulsively heated from below. Such experiments are often cited as evidence for the existence of layers in physical situations in which double-diffusive instability appears (for an astrophysical example, see Spruit 1992). However, these doubly diffusive systems may be better interpreted as instances in which an established thermal gradient is slowly increased beyond the critical threshold of instability. We then expect that oscillatory convection would set in as discussed by Veronis (1968), but whether this system would form layers has not yet been investigated. The fact is that only recently have numerical simulations been able to probe the parameter regimes of interest while experiments on such an ideal situation are quite difficult to set up.

Biello (1996) discusses an attempt at such an experiment. The apparatus took the form of a tall, thin slot filled with water with a vertical salt gradient. The idea was to suppress buoyant motions induced by horizontal temperature differences by having a narrow slot, but allow for the onset of convection driven by vertical temperature gradients. Unfortunately, the experiment was dominated by layers forming from horizontal intrusions due to residual horizontal gradients across both the slot and in a

third dimension (Chen, Briggs & Whirtz 1971). The removal of these unwanted effects requires a much more careful experimental setup. Partly with an eye to conducting such improved experiments, we give here a theoretical background to the problem.

Our theoretical study consists of a linear stability analysis of double-diffusive instability in the tall, thin slot. In a sense, this is simply the usual thermohaline convection problem, but with the bounding plates rotated through 90° (see figure 1). Moreover, since any linear stability analysis is a woefully incomplete description of the dynamics of instability, we go further and derive a weakly nonlinear theory valid just beyond the threshold of instability. In fact, it is this study of the nonlinear dynamics that is the main motivation behind this article.

We show that instability typically occurs first at small vertical wavenumbers. This guides us to construct a long-wave theory for the nonlinear development of the instability. The resulting amplitude equations, what we call either the ‘*ABC* system’ or the ‘*A* system’, are different from those normally derived in convection theory (Chapman & Proctor 1980; Bretherton & Spiegel 1983). This does not mean that they are highly specific to thermohaline convection in a slot. In fact, the equations have much wider application. Most closely related are problems such as doubly diffusive convection in a porous slot (Murray & Chen 1989), which naturally possess similar dynamics. However, in general, the amplitude equations are applicable to any system for which instability sets in through long waves, but with finite frequency. The non-zero frequency sets the weakly nonlinear theory apart from previous long-wave calculations of thermohaline or binary fluid convection, which have frequency vanishing with wavenumber (Childress & Spiegel 1981; Pismen 1987). However, we note that there are various mathematical similarities of our study with the work of Proctor & Holyer (1986) who were interested in the stability of salt fingers.

Because the laboratory experiment that originally motivated this study proved to be something of a red herring, we emphasize that this is primarily a mathematical study of the weakly nonlinear dynamics of a class of problems in which instability sets in through long waves with finite frequency. The amplitude equations are not specific to thermohaline or even fluid systems, and have not previously been derived (probably because the more commonly encountered long-wave instabilities have zero frequency, or the onset of instability is at finite wavenumber). However, these equations, as we shall see, model a rich array of dynamical behaviour. As such, they provide an interesting alternative to many of the models currently used in the theory of nonlinear dynamics (notably the complex Ginzburg-Landau equation).

2. Formulation

Consider a fluid confined to a tall, thin slot and with constant gradients of temperature and salinity in the vertical direction (see figure 1). With the Boussinesq approximation to the Navier–Stokes equations, two-dimensional perturbations to the motionless, conducting state satisfy the dimensionless equations

$$\left[\frac{1}{\sigma} \partial_t - \nabla^2 \right] \nabla^2 \psi + R_T \theta_x - R_S \Sigma_x = \frac{1}{\sigma} J(\psi, \nabla^2 \psi), \quad (2.1)$$

$$[\partial_t - \nabla^2] \theta + \psi_x = J(\psi, \theta), \quad (2.2)$$

$$[\partial_t - \tau \nabla^2] \Sigma + \psi_x = J(\psi, \Sigma), \quad (2.3)$$

where ψ is the streamfunction, θ and Σ are the perturbations of temperature and salt from the background, R_T and R_S are the thermal and solutal Rayleigh numbers, respectively, σ is the Prandtl number and τ^{-1} is the Lewis number.

The equations (2.1)–(2.3) come with various boundary conditions, depending on the precise physical problem of interest. On the front and back walls, $x = 0$ and 1, no slip on the velocity field implies $\psi = \psi_x = 0$, whereas stress free gives $\psi = \psi_{xx} = 0$. If the diffusing components are fixed in value, then $\Sigma = \theta = 0$ on $x = 0$ and 1. Alternatively, if the bounding walls are impervious to diffusion, then $\theta_x = \Sigma_x = 0$ (fixed fluxes). When the walls are not perfectly impermeable to heat and salt, intermediate, ‘leaky conditions’ are $\theta_x \mp \lambda_T \theta = \Sigma_x \mp \lambda_S \Sigma = 0$ on $x = 0$ or 1. We consider various combinations of these boundary conditions in the linear stability analysis. For nonlinear theory, the important condition of the boundaries is whether they are fixed heat and salt or fixed flux (we consider the latter case in most detail). The ‘leaky’ case allows us to bridge the gap between the two cases.

Finally, since the geometry under consideration is a tall thin slot, we expect that the top and bottom boundaries should have little effect on the linear stability calculation and so we postpone their consideration until later. However, since the slot is a tall one, we envision that convective rolls can be set up on scales of the order of the thickness of the slot, and so we assume, for now, that all fields are proportional to e^{ikz} in the linear stability analysis (though it will turn out that $k = 0$ is most important).

3. Linear stability analysis

The linear problem can be written formally as

$$\mathbf{L}_k \mathbf{\Psi} \equiv \begin{bmatrix} (\sigma^{-1} \partial_t + k^2 - \partial_x^2) (\partial_x^2 - k^2) & R_T \partial_x^2 & -R_S \partial_x^2 \\ 1 & \partial_t + k^2 - \partial_x^2 & 0 \\ 1 & 0 & \partial_t + \tau k^2 - \tau \partial_{xx}^2 \end{bmatrix} \begin{pmatrix} \psi_x \\ \theta \\ \Sigma \end{pmatrix} = 0. \quad (3.1)$$

In the thermohaline problem there are two types of instabilities. Steady convection sets in through a direct instability, whereas oscillatory convection appears at a Hopf bifurcation. For $\tau \ll 1$, steady convection typically sets in for $R_T \gg R_S$, which signifies that the background state has density increasing with height. Oscillatory convection, on the other hand appears for $R_T \sim R_S$, when the density may still decrease with height. Hence, as we raise the temperature gradient (R_T), the onset of convection is usually in the form of oscillations, and this is where we direct our attention in this article.

In what follows, we fix the parameters τ and σ (for purposes of illustration we take $\tau = 0.1$ and $\sigma = 7$). The two free parameters are then the two Rayleigh numbers, R_S and R_T . On fixing one of these numbers, R_S say, we may look for states on the threshold of linear instability by varying the other, R_T ; this leads to stability boundaries, $R_T = R_{T,s}(k^2, R_S)$ for steady convection and $R_T = R_{T,h}(k^2, R_S)$ for overstability. Once these boundaries are determined, we may isolate the points at which instability first sets in as a function of wavenumber, k ; these are the marginal stability points, $R_T = R_{T,m}(R_S)$ and $k = k_m(R_S)$.

3.1. The analytical problem

The stability problem can be solved in closed form in the case in which the boundaries are stress free and the fluxes are fixed. The eigenfunctions then have the dependence

$e^{\lambda t} \cos n\pi x$, and the governing equations become

$$(\sigma^{-1}\lambda + p^2) p^2 \psi_x - n^2 \pi^2 (R_S \Sigma + R_T \theta) = 0, \quad (3.2)$$

$$(\lambda + p^2) \theta + \psi_x = 0, \quad (3.3)$$

$$(\lambda + \tau p^2) \Sigma + \psi_x = 0, \quad (3.4)$$

where $p^2 = \pi^2 n^2 + k^2$. Thus the dispersion relation is given by

$$\lambda^3 + \lambda^2 p^2 (\tau + \sigma + 1) + \lambda \left[p^4 (\sigma + \sigma\tau + \tau) + \frac{n^2 \pi^2}{p^2} \sigma (R_S - R_T) \right] + \sigma\tau p^6 + n^2 \pi^2 \sigma (R_S - \tau R_T) = 0. \quad (3.5)$$

A bifurcation to steady convection occurs when $\lambda = 0$ and (see Veronis 1968)

$$R_T = R_{T,s} \equiv \frac{R_S}{\tau} + \frac{p^6}{n^2 \pi^2}.$$

Overstable oscillations arise through a Hopf bifurcation, for which λ is purely imaginary. We set $\lambda = i\omega$ in (3.5) and obtain $R_T = R_{T,h}$ with

$$R_{T,h} \equiv \frac{\sigma + \tau}{\sigma + 1} R_S + (\sigma + \tau + \sigma\tau + \tau^2) \frac{p^6}{n^2 \pi^2 \sigma} \quad \text{and} \quad \omega^2 = \frac{\sigma(1 - \tau)}{\sigma + 1} \frac{n^2 \pi^2 R_S}{p^2} - \tau^2 p^4. \quad (3.6)$$

For fixed R_S and small τ the Hopf curve occurs at lower values of R_T than the stationary branch. Moreover, the marginal state is given by $n = 1$ and $k = 0$, with $R_T = R_{T,m}$ and $\omega = \omega_m$, where

$$R_{T,m} \equiv \frac{\sigma + \tau}{\sigma + 1} R_S + (\sigma + \tau + \sigma\tau + \tau^2) \frac{\pi^4}{\sigma} \quad \text{and} \quad \omega_m^2 \equiv \frac{1 - \tau}{\sigma + 1} \sigma R_S - \pi^4 \tau^2. \quad (3.7)$$

That is, long waves with finite frequency.

The physical interpretation of this instability is as follows. From the linear eigenfunction we observe that the velocity field is given by

$$u = -ik\psi = -\frac{ik}{n\pi} e^{\lambda t + ikz} \sin n\pi x \quad \text{and} \quad w = \psi_x = e^{\lambda t + ikz} \cos n\pi x. \quad (3.8)$$

Hence, when $k \rightarrow 0$, motion is primarily vertical. Moreover, the velocity field of the marginally stable mode ($n = 1$) takes the form of two counterflowing streams. In other words, on introduction of a buoyancy perturbation through thermal and salinity anomalies, the fluid forms a pair of adjacent columns, one ascending, one descending. The columns traverse a finite distance before thermal diffusion obliterates the temperature anomalies in the columns, which then sink or rise due to their anomalous salt content. Subsequently, the descending and ascending columns again exchange heat, regain buoyancy, and the cycle repeats. Hence the fluid forms two adjacent columns that rock up and down and out of phase.

3.2. Numerical results

For the other types of boundary conditions, the stability results are not so simply given. Instead, we employ a Newton–Raphson–Kantorovich algorithm (Cash & Singhal 1982) to solve the problem numerically. The results are shown in figures 2–4. These figures show, respectively, the cases (a) fixed fluxes and no slip, (b) fixed salt and heat with no slip and (c) fixed salt and heat with stress free. In all the cases, the onset of

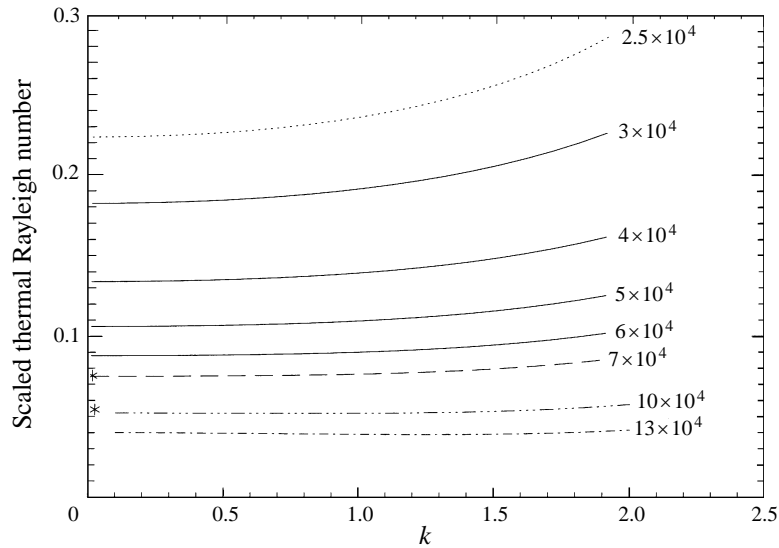


FIGURE 2. Critical Rayleigh number, scaled to that of the analytic case, $R_T(\sigma + 1)/[R_S(\sigma + \tau)] - 1$, versus vertical wavenumber. Boundary conditions correspond to fixed flux of salt and temperature and no-slip on the velocity field (case *a*). The curves are labelled by R_S . The minimum of the 10×10^4 and 13×10^4 curves do not occur at $k = 0$. Asterisks indicate the parameters used for the eigenfunctions of figures 6 and 7.

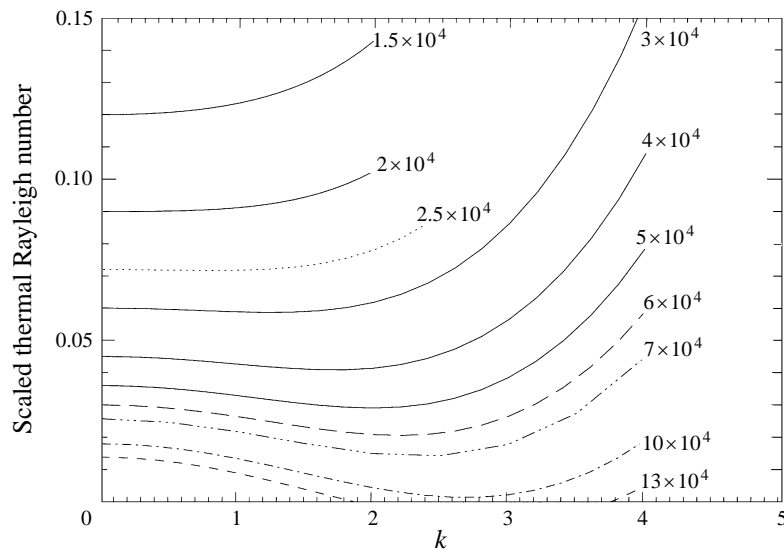


FIGURE 3. $R_T(\sigma + 1)/[R_S(\sigma + \tau)] - 1$ against vertical wavenumber for boundary conditions corresponding to fixed salt and heat with no-slip on the velocity field (case *b*). The curves are labelled by R_S .

steady convection occurs for higher thermal Rayleigh numbers than the inception of oscillations; the stability boundaries of the oscillatory modes are pictured. Moreover, we have normalized to the thermal Rayleigh number for instability in the case of stress free and fixed flux of solute and temperature.

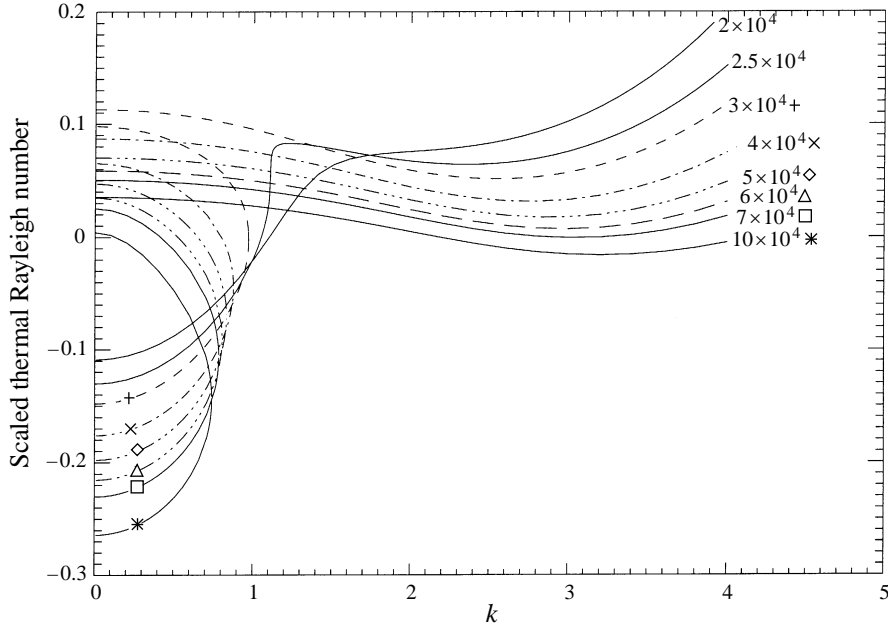


FIGURE 4. $R_T(\sigma+1)/[R_S(\sigma+\tau)]-1$ versus vertical wavenumber for fixed salt and heat with stress-free boundaries (case *c*). The curves are labelled by R_S . Note that the stability boundary for fixed R_S is not simply connected, the lower region which is not asymptotic to the analytic case is referred to as the isola.

In figure 5 we also show the corresponding frequencies at which the oscillatory bifurcations occur in case (*a*). The main point to note from this figure is that as $k \rightarrow 0$, the frequency again remains finite, a feature which proves vital in the nonlinear theory. Lastly, figures 6–8 show a selection of marginal eigenfunctions.

Although the modal dispersion relation cannot be constructed in closed form if the boundary conditions are other than fixed flux and stress free, when R_S is large and $k \rightarrow 0$ we can simplify the linear problem by asymptotic means. In this limit, the analytical solution suggests the scalings, $R_T \sim R_S$, $\omega^2 \sim R_S$, $\psi \sim R_S^{1/2}\theta$ and $\Sigma \sim \theta$. Hence, to the leading two orders in R_S^{-1} , equations (2.1)–(2.3) become

$$i\omega\sigma^{-1}\psi_{xx} + R_T\theta_x - R_S\Sigma_x \approx \psi_{xxxx}, \quad (3.9)$$

$$i\omega\theta + \psi_x \approx \theta_{xx}, \quad (3.10)$$

$$i\omega\Sigma + \psi_x \approx \tau\Sigma_{xx}, \quad (3.11)$$

where the right-hand sides are small. A regular expansion then gives the asymptotes of the stability boundaries,

$$R_{T,h} \approx \frac{\sigma + \tau}{1 + \sigma} R_S \quad \text{and} \quad \omega^2 \approx \frac{\sigma(1 - \tau)}{\sigma + 1} R_S. \quad (3.12)$$

To extract the dominant variation of the stability boundaries with R_S , we show the departure of R_T and ω from these asymptotic values in the figures; that is, $(1 + \sigma)R_{T,h}/[(\sigma + \tau)R_S] - 1$ and $(1 + \tau)\omega^2/[(1 - \tau)\sigma R_S] - 1$.

This asymptotic calculation proceeds in a regular fashion if the leading-order eigenfunctions, $\psi \sim i\omega\theta \sim i\omega\Sigma$, satisfy the boundary conditions. This is the case for the combinations stress free and fixed flux and no slip and fixed values. If

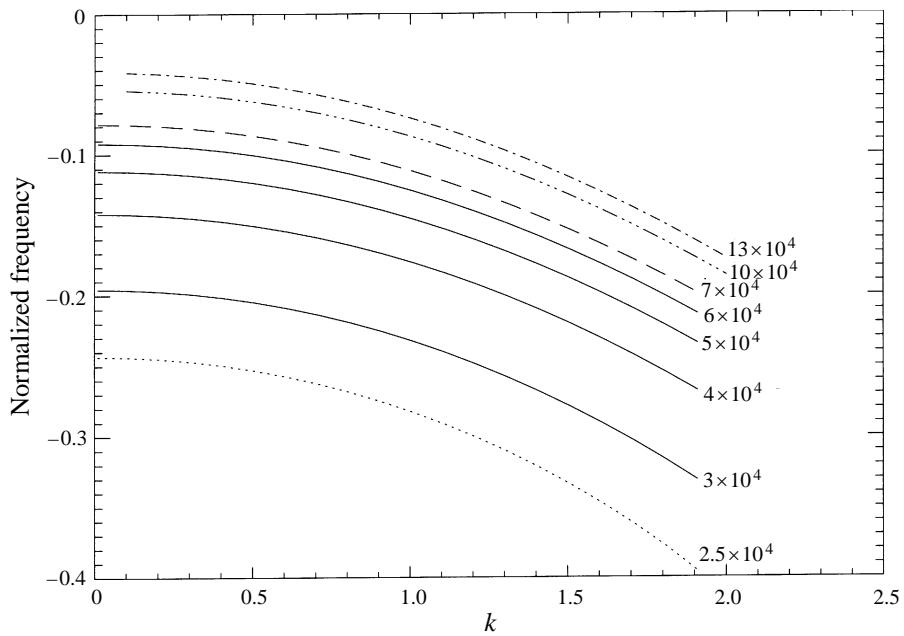


FIGURE 5. $\omega^2(\sigma + 1)/[\sigma R_S(1 - \tau)] - 1$ versus vertical wavenumber for fixed flux and no-slip (case *a*). The curves are labeled by R_S .

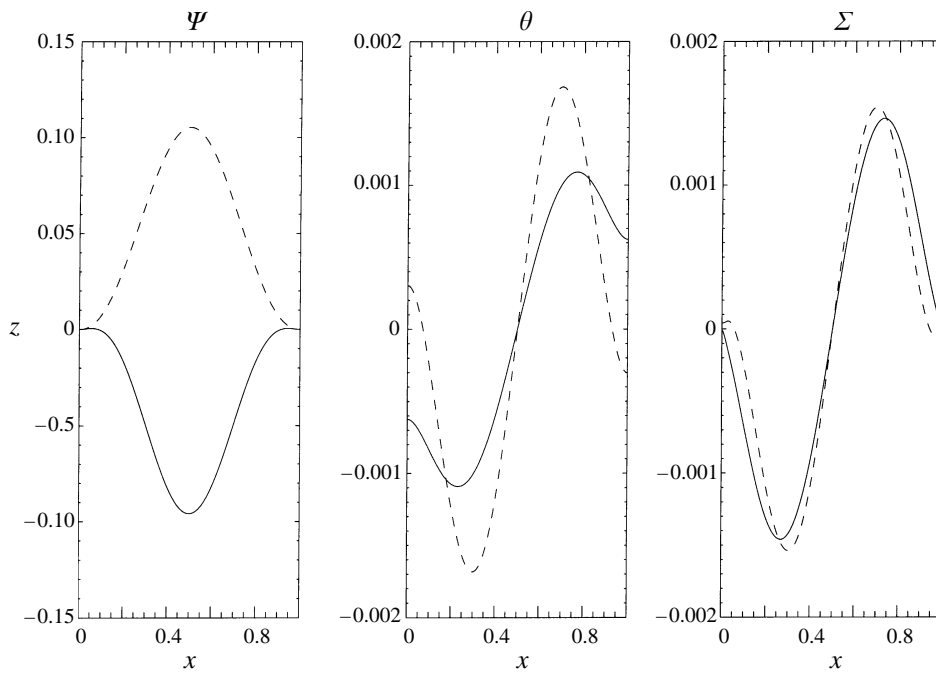


FIGURE 6. Real (solid curves) and imaginary (dashed curves) parts of the stream function, temperature and salt fields, respectively, versus x for $R_S = 7 \times 10^4$ at $k = 0$. This is the marginal eigenfunction for the case of fixed flux and no-slip boundaries (case *a*).

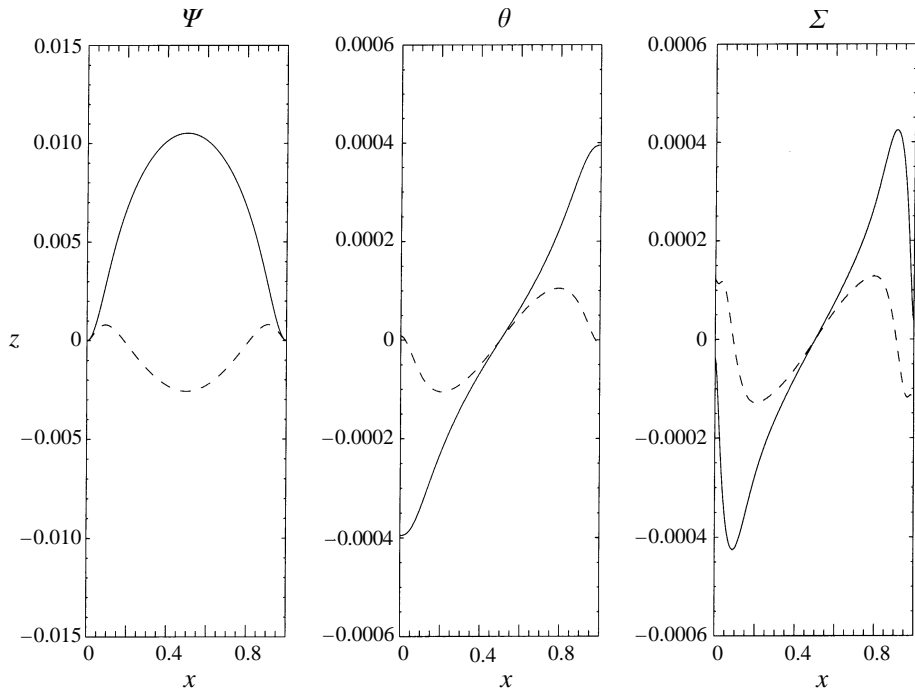


FIGURE 7. Real and imaginary parts of the stream function, temperature and salt fields, respectively, versus x for $R_S = 10^5$ at $k = k_{min} \neq 0$. The recirculation cells at the boundaries are necessary in order to fit the boundary conditions (fixed flux and no-slip; case *a*) and this effect causes the instability to set in at $k \neq 0$ for large R_S .

the boundary conditions are anything other than these two combinations, then the leading-order solution fails, suggesting the presence of boundary layers near the walls. Indeed, the eigenfunctions shown in figures 7 and 8 exhibit such features.

Over significant ranges of salt Rayleigh number, for all four sets of boundary conditions, the points of marginal stability occur at $k = 0$. However, an interesting feature of the problem with no-slip boundaries is that when R_S is sufficiently large, the marginal wavenumber is not zero (cases *a* and *b*; figures 2 and 3). This feature appears to be connected to the development of recirculation cells near the walls that preserve the no-slip condition (figure 7). As R_S increases, these recirculations must be responsible for long waves becoming less preferable than finite-wavenumber rolls.

The stability boundaries for the third case (fixed value and stress free), show more unusual features. As R_S increases, the stability boundary pinches off and an isola is created near $k = 0$ (figure 4). Importantly, for the isola, $k = 0$ remains the marginal value. The formation of this isola is symptomatic of thermal and saline boundary layers developing in the eigenfunctions (see figure 8). Stability boundaries with similar features have previously been found for triply diffusive fluids (Pearlstein 1981).

In principle, we could study the linear problem in further detail in order to understand more of the physics underlying the unusual features of the stability boundaries. However, we now leave linear stability and discuss weakly nonlinear theory. More specifically, we look for long-wave, finite-amplitude solutions. Hence a remark about cases when $k = 0$ is not marginal is in order. In the circumstance that finite-wavenumber rolls are preferred at onset, the development of mildly unstable rolls

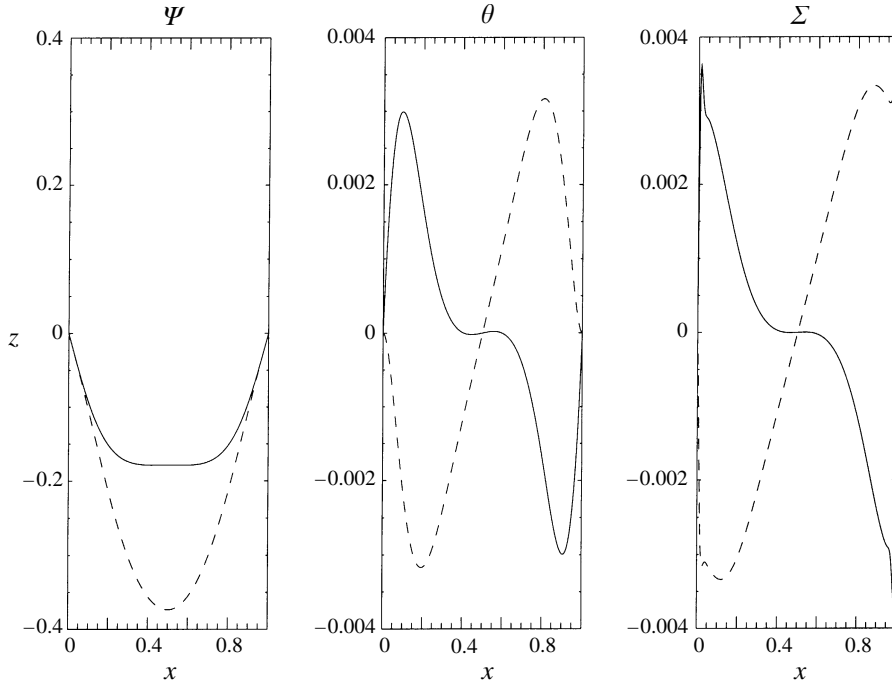


FIGURE 8. Real and imaginary parts of the stream function, temperature and salt fields versus x for $R_S = 4 \times 10^4$ at $k = 0$. This is the marginal eigenfunction for the case of stress-free and fixed salt and temperature (case c): the isola. Note the sharp boundary layers in the salt and temperature.

is described by a complex Ginzburg-Landau equation (see Bretherton & Spiegel 1983). The dynamics of extended systems described by such equations has been extensively explored in the past (e.g. Chaté 1994) and for this reason we ignore the possibility of such finite-wavenumber instability in the weakly nonlinear development. The results described above indicate the physical regimes in which the long-wave expansion is justified.

4. Weakly nonlinear expansion

The linear stability analysis of the previous section indicates that over significant regions of parameter space, convection in the slot develops at zero vertical wavenumber. We now go further and derive associated long-wave equations. We take a small parameter, ϵ , as the measure of the supercriticality of the instability. Hence we fix R_S and set $R_T = R_0 + \epsilon^2 R_2$ where $R_0 = R_{T,m}$ is the marginal Rayleigh number. To capture slowly developing long waves, we introduce the second, slow timescale, $T = \epsilon^2 t$, and the long length scale, $Z = \epsilon z$. With these scalings, the equations become

$$\frac{1}{\sigma} \psi_{xxt} - \psi_{xxxx} + R_0 \theta_x - R_S \Sigma_x = \epsilon \frac{1}{\sigma} J(\psi, \psi_{xx}) - \epsilon^2 \left(\frac{\psi_{xxT} + \psi_{ZZt}}{\sigma} - 2\psi_{xxZZ} + R_2 \theta_x \right), \quad (4.1)$$

$$(\partial_t - \partial_x^2) \theta + \psi_x = \epsilon J(\psi, \theta) + \epsilon^2 (\partial_Z^2 - \partial_T) \theta, \quad (4.2)$$

$$(\partial_t - \tau \partial_x^2) \Sigma + \psi_x = \epsilon J(\psi, \Sigma) + \epsilon^2 (\tau \partial_Z^2 - \partial_T) \Sigma, \quad (4.3)$$

to $O(\epsilon^4)$, where the Jacobian is now defined with Z .

4.1. The analytical case

We first consider the analytical case; that is, stress-free, fixed-flux boundary conditions. We pose the asymptotic series

$$\psi = \epsilon\psi_1 + \epsilon^2\psi_2 + \dots, \quad \theta = \epsilon\theta_1 + \epsilon^2\theta_2 + \dots, \quad \Sigma = \epsilon\Sigma_1 + \epsilon^2\Sigma_2 + \dots, \quad (4.4)$$

introduce these relations into the equations, and organize the various terms into an asymptotic hierarchy which we solve order by order. At leading order we find

$$\sigma^{-1}\psi_{1xx} - \psi_{1xxx} + R_0\theta_{1x} - R_S\Sigma_{1x} = 0, \quad (4.5)$$

$$(\partial_t - \partial_x^2)\theta_1 + \psi_{1x} = 0 \quad \text{and} \quad (\partial_t - \tau\partial_x^2)\Sigma_1 + \psi_{1x} = 0. \quad (4.6)$$

These relations are just the linear equations for the marginal mode; a solution is

$$\begin{pmatrix} 1 \\ -1/(\pi^2 + i\omega) \\ -1/(\tau\pi^2 + i\omega) \end{pmatrix} [A(Z, T)e^{i\omega t} + \text{c.c.}] \cos \pi x, \quad (4.7)$$

where $\omega = \omega_m$ is given in equation (3.7). However, this is not the only solution. The two solutions, $\theta_1 = B(Z, T)$ with $\psi_1 = \Sigma_1 = 0$, and $\Sigma_1 = C(Z, T)$ with $\psi_1 = \theta_1 = 0$, are also possible. These are simply the perturbations to the mean heat and salt fields. In fact, to obtain the correct nonlinear amplitude equations it is vital to introduce all three solutions at leading order. Hence we take

$$\begin{pmatrix} \psi_{1x} \\ \theta_1 \\ \Sigma_1 \end{pmatrix} = \begin{pmatrix} 1 \\ -1/(\pi^2 + i\omega) \\ -1/(\tau\pi^2 + i\omega) \end{pmatrix} [Ae^{i\omega t} + \text{c.c.}] \cos \pi x + \begin{pmatrix} 0 \\ 1 \\ 0 \end{pmatrix} B + \begin{pmatrix} 0 \\ 0 \\ 1 \end{pmatrix} C, \quad (4.8)$$

where A , B and C are unknown amplitudes depending on Z and T and which become known through the desired long-wave equations. Note that A is complex, but B and C are real.

At $O(\epsilon^2)$ we again find linear equations. These need not be considered and we move onto order ϵ^3 . At this order, the equations are

$$\frac{1}{\sigma}\psi_{3xxt} - \psi_{3xxxx} + R_0\theta_{3x} - R_S\Sigma_{3x} = \left[\frac{\pi^2}{\sigma}A_T - \left(2\pi^2 + \frac{i\omega}{\sigma} \right) A_{ZZ} - \frac{\pi^2 R_2}{\pi^2 + i\omega} A \right] e^{i\omega t} \cos \pi x, \quad (4.9)$$

$$\theta_{3t} - \theta_{3xx} + \psi_{3x} = \left(\frac{A_T - A_{ZZ}}{\pi^2 + i\omega} + AB_Z \right) e^{i\omega t} \cos \pi x - B_T + B_{ZZ} - \frac{\pi^2}{\pi^4 + \omega^2} |A|_Z^2 + \text{o.t.}, \quad (4.10)$$

$$\Sigma_{3t} - \tau\Sigma_{3xx} + \psi_{3x} = \left(\frac{A_T - \tau A_{ZZ}}{\tau\pi^2 + i\omega} + AC_Z \right) e^{i\omega t} \cos \pi x - C_T + \tau C_{ZZ} - \frac{\tau\pi^2}{\tau^2\pi^4 + \omega^2} |A|_Z^2 + \text{o.t.}, \quad (4.11)$$

where o.t. signifies other, uninteresting terms. To solve these equations, we must enforce solvability conditions corresponding to the three linear, marginal solutions. These solvability conditions may be written in the form

$$A_T = \gamma A + \eta A_{ZZ} - \delta AB_Z + \beta AC_Z, \quad (4.12)$$

$$B_T = B_{ZZ} - \xi |A|_Z^2, \quad (4.13)$$

$$C_T = \tau(C_{ZZ} - \alpha |A|_Z^2), \quad (4.14)$$

where

$$\eta = I^{-1} [2 + i\omega/(\pi^2\sigma) + R_0/(i\omega + \pi^2)^2 - \tau R_S/(i\omega + \tau\pi^2)^2], \quad (4.15)$$

$$\beta = I^{-1}R_S/(i\omega + \tau\pi^2), \quad \delta = I^{-1}R_0/(i\omega + \pi^2), \quad \gamma = I^{-1}R_2/(i\omega + \pi^2), \quad (4.16)$$

$$\alpha = \pi^2/(\omega^2 + \tau^2\pi^4) \quad \text{and} \quad \xi = \pi^2/(\omega^2 + \pi^4), \quad (4.17)$$

with

$$I \equiv 1/\sigma + R_0/(i\omega + \pi^2)^2 - R_S/(i\omega + \tau\pi^2)^2. \quad (4.18)$$

We will consider this system in more detail in later sections. Note that $\gamma \propto R_2$ measures the proximity of the stability boundary. That is, it is an instability, or control, parameter.

4.1.1. Leaky walls

The case of fixed fluxes is very special in that we may add any constant to the temperature and salt fields. This symmetry is the origin of the eigenmodes B and C that we have included in the nonlinear theory. However, it is both interesting and useful to break this symmetry in order to be able to connect the finite-amplitude theory to that which emerges when there are no such symmetries (see §4.2). In order to break the symmetry, whilst keeping the problem analytically tractable, we may add symmetry breaking terms as a perturbation. That is, we consider poorly conducting sidewalls that permit a small flux of salt. This is embodied in the modified boundary conditions on the sidewalls,

$$\theta_x - \epsilon^2\lambda_T\theta = \Sigma_x - \epsilon^2\lambda_S\Sigma = 0 \quad \text{on} \quad x = 0, \quad (4.19)$$

$$\theta_x + \epsilon^2\lambda_T\theta = \Sigma_x + \epsilon^2\lambda_S\Sigma = 0 \quad \text{on} \quad x = 1, \quad (4.20)$$

where λ_T and λ_S are parameters.

With the new boundary conditions, the problem is not altered at leading order. Only the order- ϵ^3 problem is affected, and when we apply the solvability condition, we obtain the modified amplitude equations

$$A_T = \hat{\gamma}A + \eta A_{ZZ} - \delta AB_Z + \beta AC_Z, \quad (4.21)$$

$$B_T = -2\lambda_TB + B_{ZZ} - \xi |A|_Z^2, \quad (4.22)$$

$$C_T = \tau \left[-2\lambda_SC + C_{ZZ} - \alpha |A|_Z^2 \right], \quad (4.23)$$

where the only coefficient as yet undefined is $\hat{\gamma}$, but this acts as our control parameter and so we omit the precise form to be concise (and drop the hat).

Equations (4.21)–(4.23) are the most general form of what we will refer to as the ‘ ABC system’.

4.2. General cases

The purpose of this subsection is to sketch out the various possibilities for the long-wave amplitude equations in the case of general boundary conditions. We include this discussion for the sake of completeness, though we will discuss only the ABC system in later sections (the reader not interested in this catalogue might wish to skip to §5). The main reason for this is that the ABC system in its most general form contains all the other long-wave equations as special cases.

We write the problem formally as $L\Psi = N(\Psi)$, in terms of a linear operator, L , and the nonlinearities, N . This equation can be solved asymptotically by posing expansions such as $\Psi = \epsilon\Psi_1 + \epsilon^2\Psi_2 + \dots$, and introducing suitable analogous sequences for the two operators. In order to solve the resulting hierarchy of equations we must again impose certain solvability conditions that generate the desired long-wave equations. This scheme depends critically on the solution of the leading-order, linear problem;

that is, on the form of the marginal modes. In the fixed-flux case that we developed analytically, there are three modes, with amplitudes A , B and C , that need to be added to the expansion. As we have already indicated, the latter two arise from an additional symmetry in the fixed-flux problem. But when there is no such symmetry, there is no corresponding neutral mode in the leading-order solution (unless we break the symmetry perturbatively). Hence we must consider the cases with different boundary conditions separately.

4.2.1. Fixed fluxes

For boundaries with fixed flux, the neutral modes B and C are present whatever the mechanical conditions. We therefore again find an ABC system, with the general form of the coefficients given by

$$\eta = \frac{1}{I} \left(2\overline{\psi_{1x}^2} + R_0\overline{\theta_1^2} - \tau R_S\overline{\Sigma_1^2} + \frac{i\omega}{\sigma}\overline{\psi_1^2} \right), \quad \beta = \frac{R_S}{I} \left(\tau\overline{\Sigma_{1x}^2} + i\omega\overline{\Sigma_1^2} \right), \quad (4.24)$$

$$\delta = \frac{R_0}{I} \left(\overline{\theta_{1x}^2} + i\omega\overline{\theta_1^2} \right), \quad \gamma = \frac{R_2}{I} \left(\overline{\theta_{1x}^2} + i\omega\overline{\theta_1^2} \right), \quad (4.25)$$

$$I = \frac{1}{\sigma}\overline{\psi_{1x}^2} + R_0\overline{\theta_1^2} - R_S\overline{\Sigma_1^2}, \quad \alpha = 2|\overline{\Sigma_{1x}}|^2, \quad \xi = 2|\overline{\theta_{1x}}|^2, \quad (4.26)$$

where overbars denote integration across the slot.

4.2.2. Fixed temperature and salt

If the salt and temperature fields are fixed on the sidewalls then the B - and C -modes do not enter the linear problem. In this circumstance, we pose a solution of the form $\Psi = \Psi_0 + \epsilon\Psi_1 + \dots$. The leading-order problem then has a solution

$$\Psi_0 = A(Z, T) \Psi^a e^{i\omega t} + \text{c.c.}, \quad (4.27)$$

with the eigenfunction Ψ^a defined from the linear theory. We then proceed to higher orders in the usual fashion; eventually we find the amplitude equation

$$A_T = \gamma A + \eta A_{ZZ} + \Gamma_1 A |A_Z|^2 + \Gamma_2 |A|^2 A_{ZZ} + \Gamma_3 A^* A_Z^2 + \Gamma_4 A^2 A_{ZZ}^*, \quad (4.28)$$

where all of the coefficients are complex. This equation is a long-wave version of the celebrated complex Ginzburg–Landau equation; we refer to it as the ‘ A system’. Some features of the system are described in the Appendix. A similar equation to (4.28) was derived by Normand (1984) in a different problem.

4.2.3. Mixed cases

The form of the amplitude equations reveals that the fixed-flux and fixed-value problems are fundamentally different. We will concentrate on the former in the coming sections, but before we go into this, we mention the cases in which fixed flux conditions are applied on one field, but fixed values on at least one boundary for the other field. This eliminates one of the linear modes, B or C . If we fix the flux on the temperature field, but set the salinity on the walls, for illustration, then the linear problem is missing the C -mode. The expansion follows that of fixed fluxes and at second order we arrive at the amplitude equations

$$A_T = \gamma A + \eta A_{ZZ} - \delta AB_Z \quad (4.29)$$

and

$$B_T = B_{ZZ} - \xi |A_Z|^2. \quad (4.30)$$

In other words, we obtain the amplitude equations of the fixed-flux problem without the C -mode. In a similar way, if we were to consider fixed salt fluxes, but fixed temperature, then the amplitude equations would again be the fixed-fluxes set, but without the B -mode. Hence the mixed boundary condition problem is a special case of the ABC system.

Equations (4.29) and (4.30) are identical to those derived by Cessi & Young (1992) for thermal convection in a tilted slot. A crucial difference, however, which makes the current system much more interesting, is that the coefficients are complex. With hindsight gained from the complex Ginzburg–Landau problem, we expect that this leads to a much richer range of dynamical behavior.

5. Limits of the amplitude equations

We now concentrate on the ABC system of equations. In its most general form, the system is

$$A_T = \gamma A + \eta A_{ZZ} - \delta AB_Z + \beta AC_Z, \quad (5.1)$$

$$B_T = -2\lambda_T B + B_{ZZ} - \xi |A|_Z^2, \quad (5.2)$$

$$C_T = \tau \left[-2\lambda_S C + C_{ZZ} - \alpha |A|_Z^2 \right]. \quad (5.3)$$

This system contains a large number of other, more well-known equations as special cases, and we devote this section to describing some of these limits.

5.1. Slaving B and C

In the limit that the parameters λ_S , λ_T , η , β , δ and γ are all small in magnitude, the system reduces to the complex Ginzburg–Landau equation. To see this, we rescale both these parameters and time by a small parameter, ε . This recasts the A -equation in its original form, but the B - and C -equations become modified to

$$\varepsilon(B_T + 2\lambda_T B) = B_{ZZ} - \xi |A|_Z^2 \quad \text{and} \quad \varepsilon(C_T + 2\lambda_S C) = \tau (C_{ZZ} - \alpha |A|_Z^2). \quad (5.4)$$

Hence to leading order in ε , we slave the B and C variables:

$$B_{ZZ} = \xi |A|_Z^2 \quad \text{and} \quad C_{ZZ} = \alpha |A|_Z^2. \quad (5.5)$$

(We proceed informally here and we do not rigorously establish the adiabatic elimination of variables.) If we integrate these equations, assume the integration constants vanish, then eliminate the slaved variables, we arrive at

$$A_T = \gamma A + \eta A_{ZZ} - (\delta \xi - \alpha \beta) |A|^2 A; \quad (5.6)$$

the Ginzburg–Landau equation. (If the integration constants do not vanish, it merely necessitates a modification of the control parameter, γ , to cast the resulting equation in this form.)

A different way of slaving B and C is to assume that the walls are relatively imperfect in imposing the no-flux condition. Then we may take $\lambda_T \gg 1$ and $\lambda_S \gg 1$. The slaving equations are then

$$2\lambda_T B = -\xi |A|_Z^2 \quad \text{and} \quad 2\lambda_S C = -\alpha |A|_Z^2, \quad (5.7)$$

from which it follows that

$$A_T = \gamma A + \eta A_{ZZ} + \left(\frac{\xi \delta}{2\lambda_T} - \frac{\alpha \beta}{2\lambda_S} \right) A |A|_{ZZ}^2. \quad (5.8)$$

This is a version of the A -system (the equation derived in §4.2.2 for the fixed-values problem).

5.2. The zero-frequency limit

Another limit of the amplitude system is when the oscillation frequency becomes very small. In the analytical problem, it is clear that this will happen if either the Prandtl number becomes small, $\sigma \ll 1$, or if $\tau \rightarrow 1$. If we set $\lambda_S = \lambda_T = 0$ and consider $\tau \rightarrow 1$, we obtain

$$\frac{1}{\sigma}A_T = \frac{R_2}{\pi^2}A + 2A_{ZZ} - \frac{R_T}{\pi^2}AB_Z + \frac{R_S}{\tau\pi^2}AC_Z, \quad (5.9)$$

$$B_T = B_{ZZ} - \frac{1}{\pi^2}|A|_Z^2 \quad \text{and} \quad C_T = \tau C_{ZZ} - \frac{1}{\tau\pi^2}|A|_Z^2. \quad (5.10)$$

In this limit, the coefficients all become real. Were we to now slave B and C as above, we would obtain the real Ginzburg–Landau equation. That equation has a Lyapunov functional and predicts evolution to the gravest mode in the system. Both this fact and the results of Cessi & Young (1992) suggest that the dynamics of the real equations (5.9)–(5.10) may be rather simple, although we cannot in general find a Lyapunov functional (though the behaviour after sufficiently long times may be relatively simple, complicated transient states may, however, appear and small perturbations can lead to richer dynamics; Balmforth 1995).

A real system like (5.9)–(5.10) was previously derived by Poyet (1981) for fixed-flux Rayleigh–Bénard convection between a pair of poorly conducting plates.

5.3. The large Rayleigh number limit

A different limit is obtained if we take the salt Rayleigh number to be large. Then both R_T and ω also become large. Once again this limit corresponds to a particular choice of the parameters of the equations. In fact,

$$\frac{2i\omega}{\sigma}A_T = R_2A - \frac{\omega^2}{\sigma\pi^2}A_{ZZ} - R_TAB_Z + R_SAC_Z, \quad (5.11)$$

$$B_T = B_{ZZ} - \frac{\pi^2}{\omega^2}|A|_Z^2 \quad \text{and} \quad C_T = \tau C_{ZZ} - \frac{\pi^2\tau}{\omega^2}|A|_Z^2. \quad (5.12)$$

Thus the system reduces to a Schrödinger-like equation, nonlinearly coupled to two diffusion equations.

This limit is analogous to one considered by Bretherton & Spiegel (1983) in the standard thermohaline problem. In that problem, one obtains the cubic Schrödinger equation at leading order. Here, the diffusive nature of the B and C modes remains and we do not obtain an integrable system unless we additionally slave B and C .

6. The ABC system

We now concentrate on the ABC system. First we put it into a ‘standard form’. Since only vertical derivatives of B and C contribute to the evolution of A , it is convenient to formulate the gradient forms of (4.13) and (4.14). Then, the number of coefficients can be decreased by rescaling the amplitudes and introducing a temporally periodic factor into A . For simplicity, we also take $\lambda_T = \lambda_S = 0$ henceforth. We use the definitions

$$\mathcal{A} = (\xi|\delta|)^{1/2}Ae^{-i\eta T}, \quad \mathcal{B} = |\delta|B_Z, \quad \mathcal{C} = |\beta|C_Z \quad (6.1)$$

Case	η	ν	μ	α
(i) Stress-free	$0.88400 + 2.4644i$	$0.68116 - 0.73213i$	$0.77685 - 0.62968i$	1.140475
(ii) No-slip	$15 + 4i$	$0.06 + i$	i	0.95

TABLE 1. Values of the coefficients of the *ABC* system. $\tau = 0.1$. Case (i) corresponds to $R_S = 4000$.

and

$$\tilde{\gamma} = \gamma_r, \quad \tilde{\alpha} = \frac{\alpha |\beta|}{\xi |\delta|}, \quad \mu = \frac{\beta}{|\beta|}, \quad \nu = \frac{\delta}{|\delta|}. \quad (6.2)$$

We further rescale the interval in Z to $[0, 1]$. After dropping tildes on all quantities, the amplitude equations are written as

$$\mathcal{A}_T = \gamma \mathcal{A} + \eta \mathcal{A}_{ZZ} - (\nu \mathcal{B} - \mu \mathcal{C}) \mathcal{A}, \quad (6.3)$$

$$\mathcal{B}_T = \left[\mathcal{B} - |\mathcal{A}|^2 \right]_{ZZ} \quad \text{and} \quad \mathcal{C}_T = \tau \left[\mathcal{C} - \alpha |\mathcal{A}|^2 \right]_{ZZ} \quad (6.4)$$

so that γ is real, and μ and ν have unit magnitude.

In subsequent sections we will solve the system of equations in some detail. We will do this for certain parameter values. The most natural choice is suggested by using the analytical formulae for the stress-free and fixed-flux problem; appropriate values for $R_S = 4000$ are listed in table 1 as case (i). We also consider an alternative set of parameters, which approximate the coefficients of the fixed-flux and no-slip problem. These are listed as case (ii) in table 1. Note that we leave the choice of γ (equivalently, R_2) open; this parameter acts as our control.

7. Equilibria and stability

In this section we shall consider equilibrium solutions of the *ABC* system and determine their stability. At this stage, however, we must specify the boundary conditions in Z ; we consider two cases.

7.1. Periodic domains

We seek periodic solutions of (6.3)–(6.4) of the form

$$\mathcal{A} = R e^{i(KZ + \Omega T)}, \quad \mathcal{B} = \mathcal{B}_0, \quad \mathcal{C} = \mathcal{C}_0 \quad (7.1)$$

where R , \mathcal{B}_0 and \mathcal{C}_0 are constants. At this stage, any constants, \mathcal{B}_0 and \mathcal{C}_0 , will suffice as solutions. Given these constants, the amplitude equations become linear in R . Hence, arbitrary \mathcal{B}_0 and \mathcal{C}_0 generate classes of solutions with undetermined amplitudes, R . In fact, these solutions are simply linear neutral modes, which are also nonlinear solutions of the periodic problem. Worse still, linear modes with Ω complex are also nonlinear solutions; neutral, exponentially growing or decaying alike. This signifies that the system is either stable, and everything decays to the trivial background state, or that the system is unstable and disturbances grow without saturation. This state of affairs is completely unsatisfactory and indicates that the *ABC* system is of questionable physical significance when solved on periodic domains.

However, there are certain solutions that correspond to the finite-amplitude solutions of the complex Ginzburg–Landau equation and it is interesting to study them for purposes of comparison and because they convey a certain amount of insight into

the general problem. This subset of solutions is obtained on taking

$$\left. \begin{aligned} \mathcal{B}_0 &= R^2, & \mathcal{C}_0 &= \alpha R^2, \\ \gamma &= \eta_r K^2 + A_r R^2, & \Omega &= -\eta_i K^2 - A_i R^2, \end{aligned} \right\} \quad (7.2)$$

where

$$A \equiv v - \mu\alpha. \quad (7.3)$$

This is a family of exact solutions to the amplitude equations with $R(K)$ and $\Omega(K)$ given implicitly by equation (7.2). Solutions therefore bifurcate supercritically or subcritically depending on the sign of the parameter A_r .

Note that in the analytical problem $A_r = 0$, implying that the periodic solutions must bifurcate vertically at the point of instability. This results from a special symmetry of this specific problem when the boundaries are stress free (Bretherton & Spiegel 1983). It indicates that one might need to proceed in the expansion, retaining higher-order terms, to find the correct nonlinear saturation term. The cubic coefficient, however, is not purely imaginary for the other possible boundary conditions. Moreover, in bounded domains, the solutions branches do not bifurcate vertically for the analytical problem. Hence cases with $A_r = 0$ do not present a failing of the theory.

In the cases we have considered, v_r and $\alpha\mu_r$ are both positive. Hence the B -mode is nonlinearly stabilizing, whereas C is destabilizing. This reflects the usual roles played by the heat and salt perturbations; the modification to the background temperature gradient by the convective heat flux stabilizes the system, but the erosion of the stabilizing salt gradient by the convective salt flux promotes further instability.

We now consider perturbations about the solution (7.2):

$$\mathcal{A} = [R + r(Z, T)] e^{i(KZ + \Omega T + \phi(Z, T))}, \quad \mathcal{B} = \mathcal{B}_0 + b(Z, T), \quad \mathcal{C} = \mathcal{C}_0 + c(Z, T), \quad (7.4)$$

with $(r, \phi, b, c) \propto e^{K^2 \lambda T + iKqZ}$, where λ and q are a suitably scaled growth rate and wavenumber, respectively. The resulting eigenvalue equation is

$$\left| \begin{bmatrix} \lambda + \eta_r q^2 + 2i\eta_i q & -\eta_i q^2 + 2i\eta_r q & v_r P & -\mu_r P \\ \eta_i q^2 - 2i\eta_r q & \lambda + \eta_r q^2 + 2i\eta_i q & v_i P & -\mu_i P \\ -2Pq^2 & 0 & \lambda + q^2 & 0 \\ -2\tau\alpha P q^2 & 0 & 0 & \lambda + \tau q^2 \end{bmatrix} \right| = 0, \quad (7.5)$$

where $P = R/K$.

If $P \ll 1$, then the dispersion relation always has a single root that for sufficiently small q is positive: $\lambda \sim 2\eta_r q$. Hence, near onset, the rolls are always unstable. Depending on parameter values, rolls can either remain unstable for all P , or becomes stable once P reaches some critical threshold, $P = P_{crit}$. We may rewrite this condition as

$$\gamma > (\eta_r + A_r P_{crit}^2) K^2, \quad (7.6)$$

which can be compared with the condition for the existence of the equilibrium solutions: $\gamma > \eta_r K^2$. These two conditions define parabolas on the (K, γ) -plane, and the situation is much the same as in Eckhaus instability theory: provided $A_r P_{crit}^2 > 0$, rolls sandwiched between the two parabolas are unstable. One point of difference, however, is that the instability invariably is oscillatory (cf. Janiaud *et al.* 1992).

7.2. Finite domains

Periodic solutions have the unappealing feature of permitting uncontrolled linear instability at worst, and being contrived at best. In this subsection we remedy

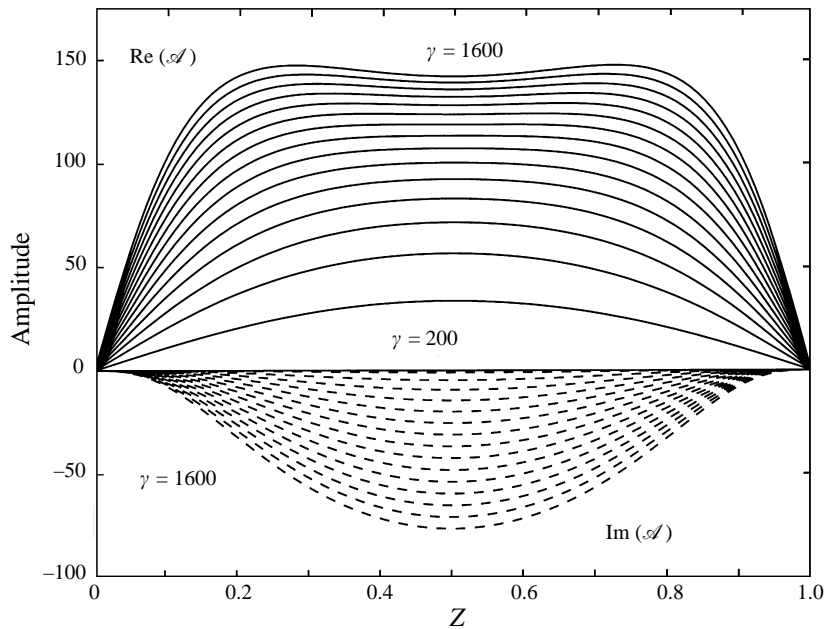


FIGURE 9. Equilibrium solutions for \mathcal{A} for increasing γ . Parameter values as in table 1, case (ii).

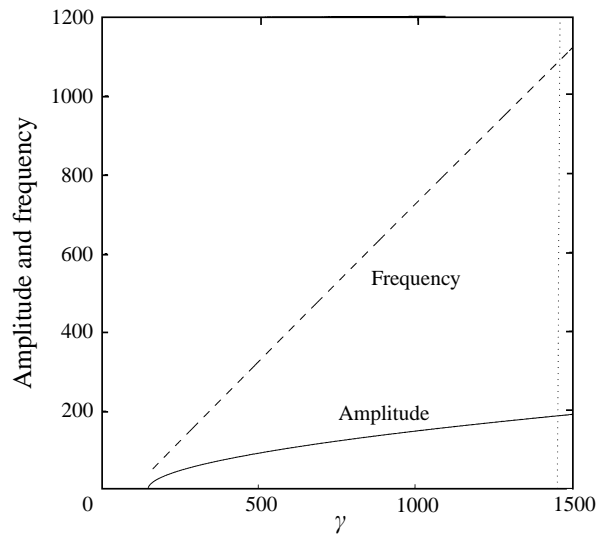


FIGURE 10. The bifurcation diagram for secondary instability of the lowest mode of the equilibrium solution and the corresponding $\Omega(\gamma)$. Beyond the dotted line the solution is unstable. The ‘amplitude’ is the average of $|\mathcal{A}|^2$ over the slot.

the situation by considering the more realistic case in which we impose boundary conditions at the bottom and top of the slot. More specifically, we consider the conditions $\mathcal{A}(0) = \mathcal{B}(0) = \mathcal{C}(0) = \mathcal{A}(1) = \mathcal{B}(1) = \mathcal{C}(1) = 0$.[†] The equation to be

[†] This choice corresponds to no motion and fixed fluxes at the upper and lower boundaries. We could alternatively apply fixed heat or salt or both, but the results are unlikely to be very different. Perhaps more seriously, the conditions are always stress-free. The asymptotic analysis does not allow

solved is

$$i\Omega\mathcal{A} = \gamma\mathcal{A} + \eta\mathcal{A}_{ZZ} - (v - \alpha\mu)|\mathcal{A}|^2\mathcal{A}, \quad (7.7)$$

where we allow for a continual rotation of the phase of \mathcal{A} ($\Omega \neq 0$). Except in certain special cases, the solutions cannot be given in closed form and we resort to numerical evaluation. From a formal point of view, the equilibrium problem is identical to that for the complex Ginzburg–Landau equation (cf. van Saarloos & Hohenberg 1994) though the secondary instability problem is not.

To construct the equilibria we introduce a Fourier sine series for the amplitudes A , B_Z and C_Z . The solution then follows from Newton iteration, with the frequency Ω determined as an eigenvalue. This scheme also has the advantage of reducing the problem of the secondary instability of these equilibria to a simple matrix eigenvalue problem.

In the finite domain, finite-amplitude solutions bifurcate from the trivial background state once γ exceeds a threshold. These points of bifurcation are given by $\gamma = \gamma_n = n^2\pi^2\eta_r$. At these parameter values, finite-amplitude solutions appear corresponding to the linear modes, $\sin n\pi Z$, of the background state. For the parameter ranges we have examined, the $n = 1$ solution bifurcates supercritically, and so one of the finite-amplitude states is, at least initially, stable.

Figure 9 shows the $n = 1$ solution at various values of the control parameter, γ , beyond threshold for parameter values of the no-slip problem (case (ii) in table 1). A bifurcation diagram showing amplitude (that is, the average of $|\mathcal{A}|^2$ over the domain) and frequency, Ω , against γ is shown in figure 10. The locus of the $n = 1$ solutions is not very remarkable. However, as indicated in the figure, the solution loses stability in a secondary bifurcation near $\gamma = 1430$.

More solutions are shown in figure 11, which shows equilibria corresponding to $n = 1-4$ at $\gamma = 1000$. The higher-order solutions ($n > 1$) are all unstable to perturbations with lower wavenumber. (However, this is not always the case for general parameter values.)

Figures 12 and 13 show solutions for the stress-free problem with various values of R_S . As we increase R_S , the solution branches bifurcate more and more sharply; at larger values of R_S , this behaviour is extreme and the bifurcation occurs almost vertically.

The solutions branches again suffer the onset of secondary instability; this is particularly severe at larger R_S , where the windows in γ over which the branches are stable become very small indeed (see figure 13). When we allow R_S to vary as a second parameter, we find the border of secondary instability in the (R_S, γ) -plane as shown in figure 14. The peculiar shape of the curve in the figure arises because of competition between different modes of secondary instability. At larger R_S , the competition is typically amongst different pairs of oscillatory modes. These lead to Hopf bifurcations, the ramifications of which we will explore in the next section. For smaller R_S , the leading secondary instabilities are direct; these instabilities correspond to ‘mixed modes’ that generate new equilibria which connect the $n = 1$ solution branch to the $n > 1$, higher-order equilibrium solutions.

for no-slip conditions at $Z = 0$ and 1. To include this additional physics we would need to place boundary layers near the upper and lower walls, find a locally valid solution there and match this with the solutions to the ABC system. This kind of problem is also encountered in the usual thermohaline problem whenever realistic horizontal boundaries are included.

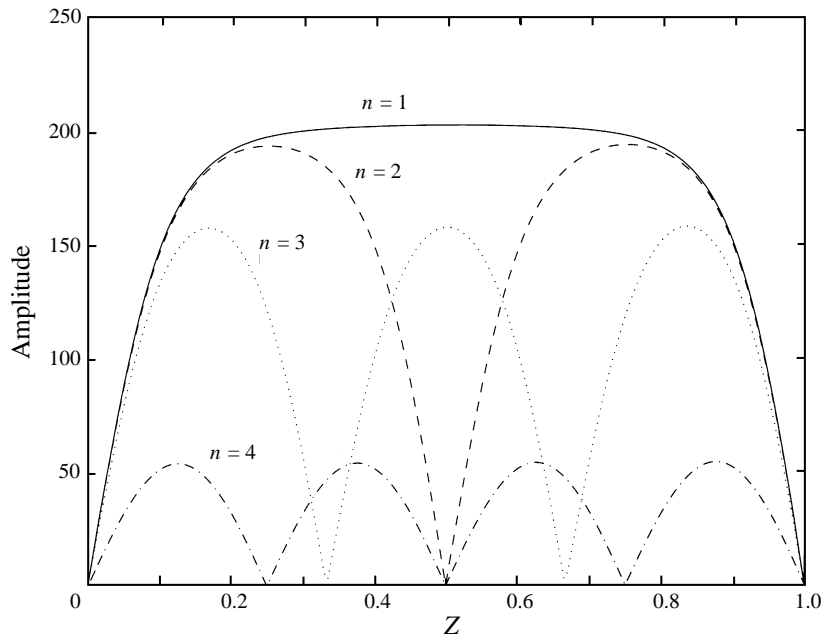


FIGURE 11. Various equilibrium solutions at $\gamma = 1000$ corresponding to the unstable modes, $\sin n\pi Z$ with $n = 1, 2, 3, 4$ of the trivial state $\mathcal{A} = 0$. The $n = 1$ to $n = 3$ solutions correspond to the patterns shown in figure 1.

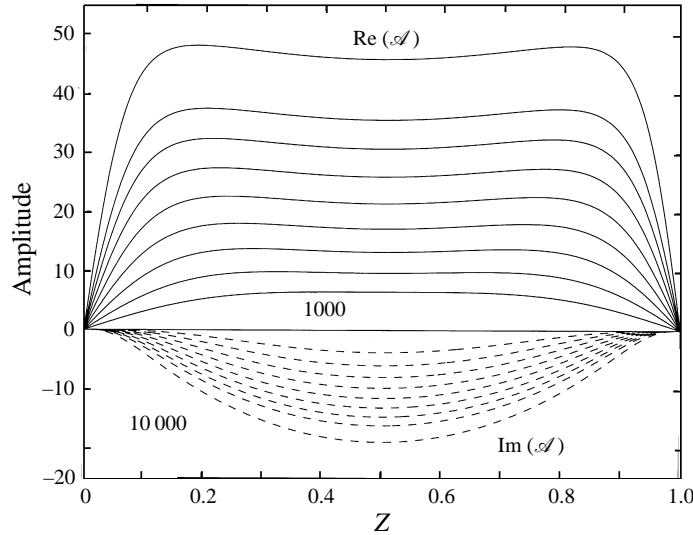


FIGURE 12. Equilibrium solutions for \mathcal{A} in the stress-free case, for $\gamma = 15$ and various values of R_S from 1000 to 10000 in steps of 1000.

8. Numerical time integrations

The equilibria described in the last section illustrate some of the possible solutions to the ABC system. Now we go further in exploring the system and solve the partial differential equations numerically with boundary conditions, $\mathcal{A} = \mathcal{B} = \mathcal{C} = 0$ on $Z = 0$ and 1. To do this we used two different schemes (one based on a

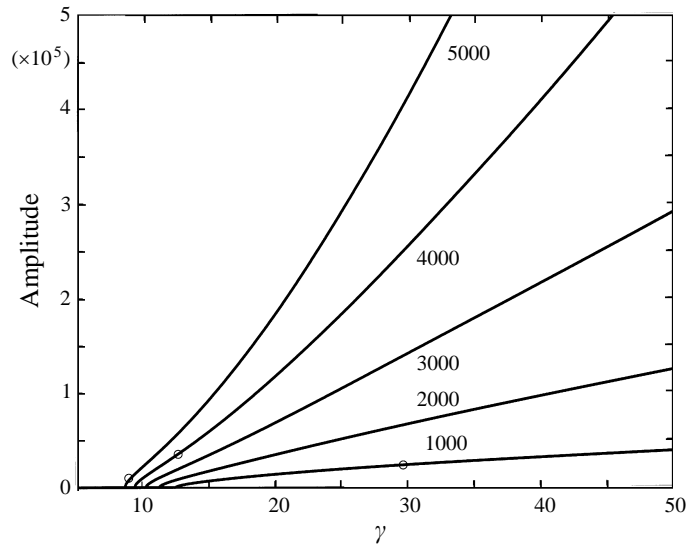


FIGURE 13. Bifurcation diagram for the analytical case. Shown are the amplitude of the equilibrium solutions for $R_S = 1000$ to 5000 in steps of 1000 . The circles show the location of the onset of secondary instability.

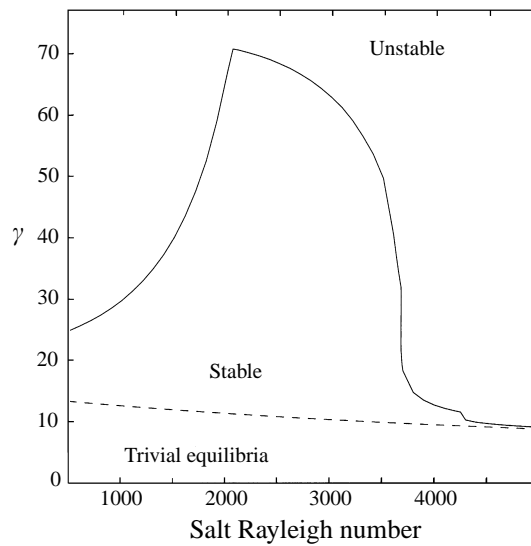


FIGURE 14. Stability boundary in the (R_S, γ) -plane for the stress-free, analytical problem. Below the dashed line, the only equilibrium solution is the trivial state $\mathcal{A} = 0$.

finite-difference algorithm, the other a finite-element collocation scheme) and verified agreement between the two. For illustration, we take the two cases listed in table 1. These lead to two different types of behaviour that we illustrate below.

8.1. Case (i): states of spatio-temporal complexity

For the stress-free (analytical) problem, there are stable equilibrium states for γ up to about 12.7 . At that value of the control parameter, secondary instability appears in the form of a Hopf bifurcation. In figure 15 we show time traces of the solution at

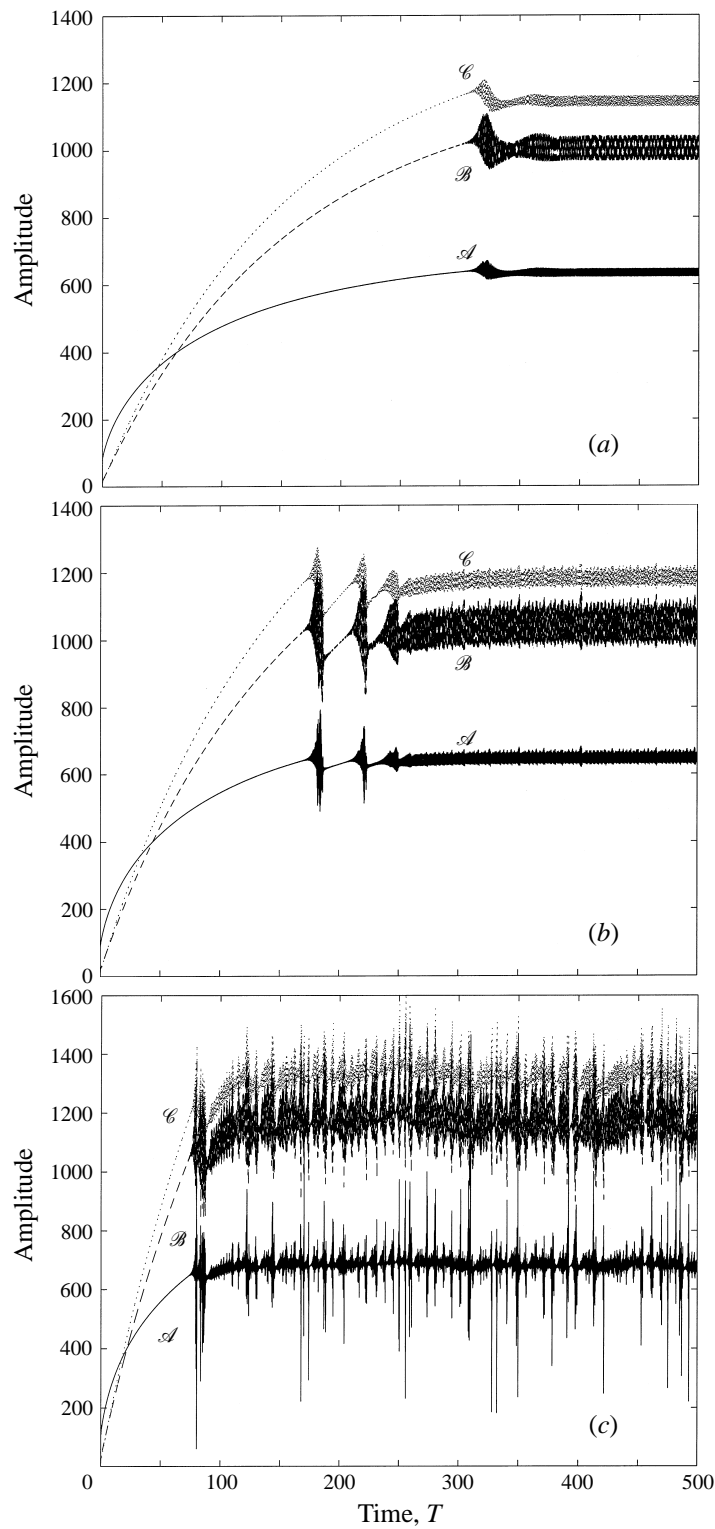


FIGURE 15. Time traces at the centre of the slot for (a) $\gamma = 13.5$, (b) $\gamma = 15$ and (c) $\gamma = 20$. The solid curves show $20 \times |\mathcal{A}(0.5, T)|$, the dashed curves $\mathcal{B}(0.5, T)$ and the dotted curves $\mathcal{C}(0.5, T)$.

the centre of the slot for $\gamma = 13.5, 15$ and 20 . Space–time surface plots of the solution for $\mathcal{B}(Z, T)$ are displayed in figure 16 in the three cases.

Just beyond the bifurcation, a stable temporally periodic solution appears (figure 16*a*), indicating the Hopf bifurcation is supercritical. For larger γ , the solutions become irregular (figures 16*b*). The transition between the two types of behaviour lies close to $\gamma = 14.36$, and appears to take the form of the familiar period-doubling cascade. We therefore conjecture that the system becomes chaotic for $\gamma > 14.36$.

For the largest value of γ , the solution undergoes erratic large-amplitude pulses amid a more regular, though still chaotic, phase (figure 16*c*). In these chaotic states, the fields evolve by ‘sloshing’ up and down the slot; that is, convection begins at the top of the slot (say), then propagates down to the lower end, then back up to the top in a relatively erratic fashion.

8.2. Case (ii): bursting states

According to equilibrium stability theory, for the no-slip problem, a stable branch of finite-amplitude solutions bifurcates from the trivial state when γ reaches $\eta_r \pi^2 \approx 150$. This branch of solutions eventually loses stability near $\gamma = 1430$ (see figure 10). In the range $[150, 1430]$ we therefore anticipate that the system relaxes to an oscillatory convective pattern like that of figure 1. This view was at least partially confirmed by direct integrations of the *ABC* system; oscillatory patterns corresponding to the equilibria of §7 were observed over this range in γ . However, the system also showed a sensitivity to initial conditions, and the equilibrium solutions were not the only states to which the system evolved.

For γ above 500, the system also showed evolution to a second, time-dependent attractor. This is illustrated in figure 17, which shows time traces and phase portraits at the slot centre. In the case shown by solid lines, the stable equilibrium solution is the ultimate end-point of evolution, but in the case drawn as dotted lines, with different initial conditions, the system has a different fate. The new attractor has the form of a bursting periodic cycle.

The origin of the periodic cycle can be roughly understood as follows. For small amplitude in \mathcal{A} and large γ , the fields \mathcal{B} and \mathcal{C} remain approximately constant (or at least slowly decay diffusively). In this situation, the \mathcal{A} -equation is essentially linear and we may decompose the field into Fourier components. This indicates that the gravest component of \mathcal{A} , $A_1 \sin \pi Z$, begins to grow exponentially. Eventually, this component excites the \mathcal{B} and \mathcal{C} fields, which then also grow exponentially in response. When nonlinearity becomes sufficiently important, this feeds back into the \mathcal{A} -equation, causing \mathcal{A} to abruptly decrease superexponentially. This returns the system to low amplitude in \mathcal{A} and the cycle repeats. This kind of behaviour is familiar from the dynamics of coupled oscillators (Cessi, Spiegel & Young 1990).

Phase portraits of the bursting cycles are shown in figure 18. One interesting feature of the cycle is that it is doubly looped. That is, one might identify it as ‘period-2’. We have not attempted to follow the orbit in parameter space and identify where this cycle originates. The cycle is also interesting in view of the additional ‘wiggles’ that develop in the orbit as we raise γ . This suggests that the orbit is becoming attracted to an object like a saddle focus, and is beginning to wind around its stable manifold. The dynamics of the system that this suggests (e.g. Balmforth 1994) is provocative, but we will not go further in exploring this here.

The two attractors continue to co-exist as we raise γ further. Eventually, however, both appear to lose stability. At $\gamma = 1430$, the equilibrium solution loses stability in a Hopf bifurcation. This bifurcation is apparently supercritical (see figure 19), and

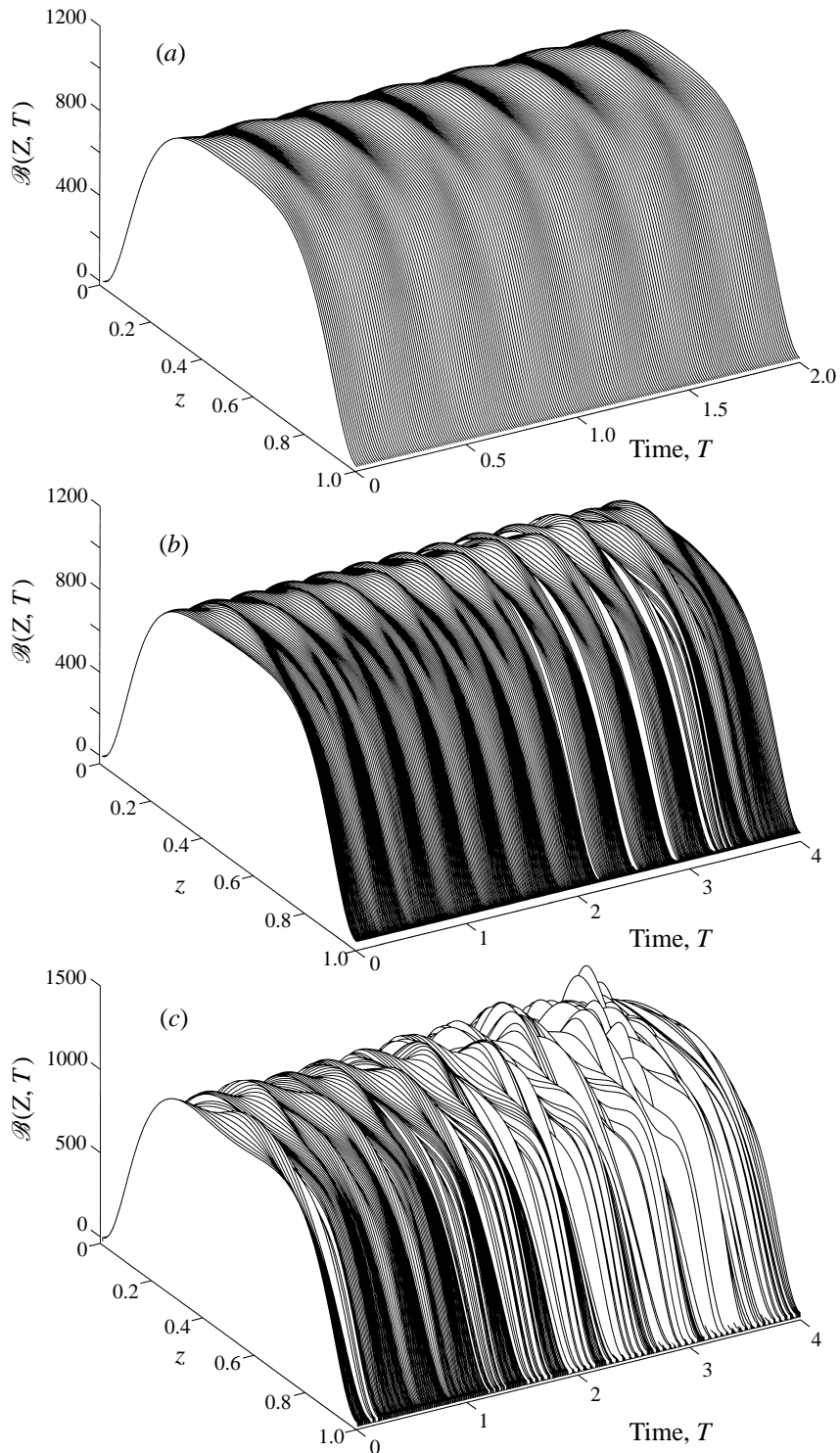


FIGURE 16. Surface plots above the (Z, T) -plane of the solution for $\mathcal{B} \equiv B_Z$, in the cases (a) $\gamma = 13.5$, (b) $\gamma = 15$ and (c) $\gamma = 20$.

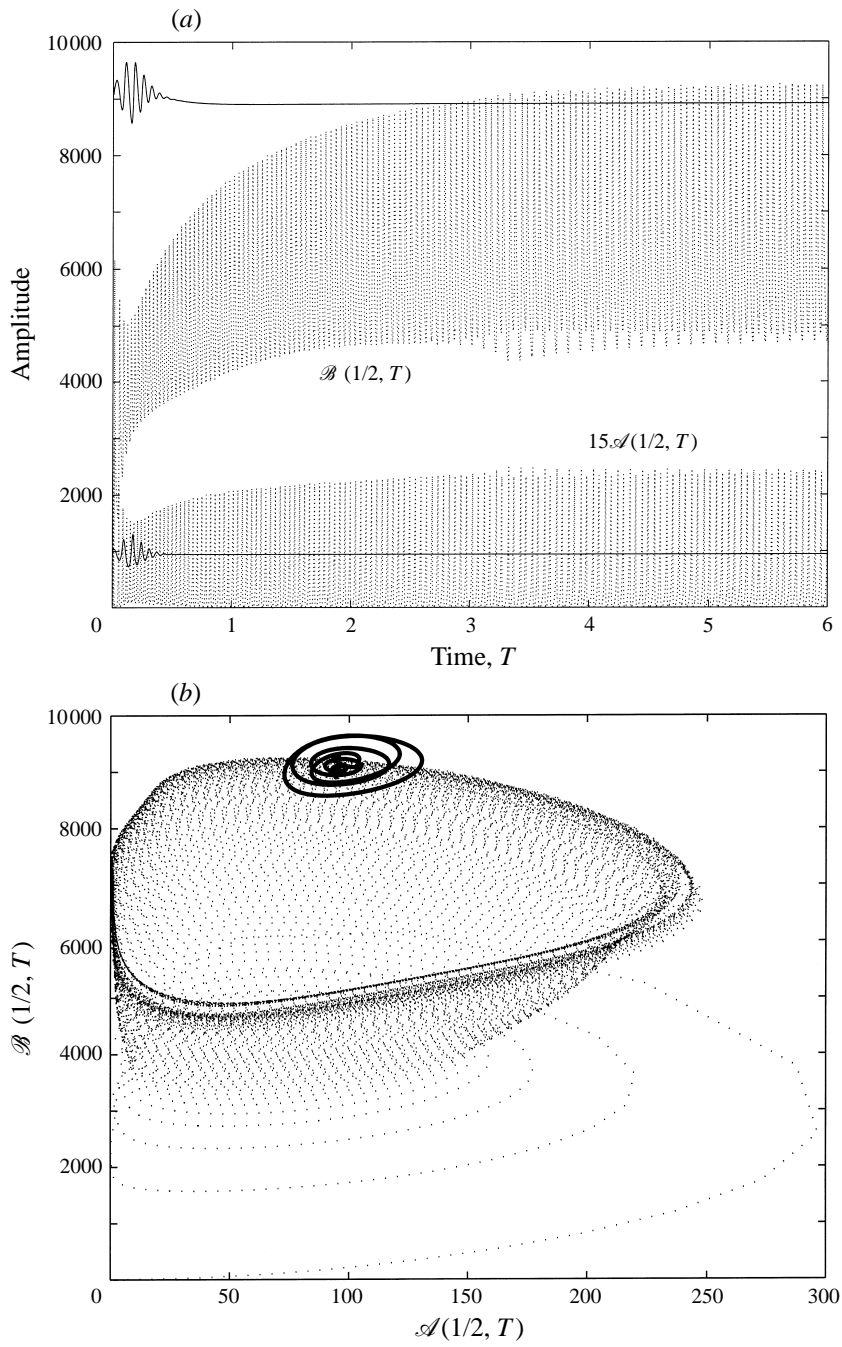


FIGURE 17. (a) Time series and (b) phase portrait projected onto the $(|\mathcal{A}|, \mathcal{B})$ plane at slot centre with $\gamma = 600$ and for two different initial conditions. The solid lined orbit converges to a fixed point while the dotted orbit converges to a limit cycle (the bursting state).

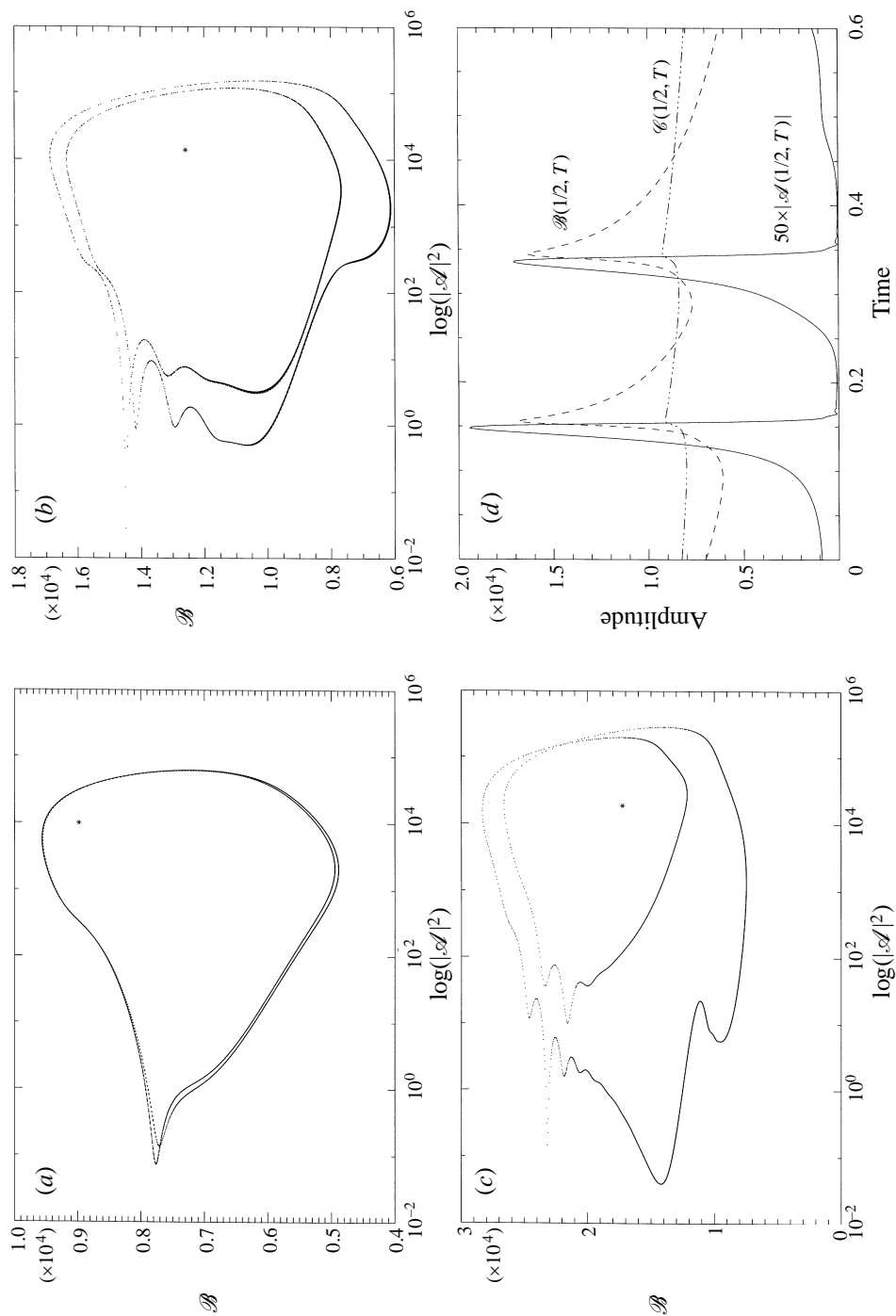


FIGURE 18. Phase portraits projected onto the $(\log|\mathcal{A}|^2, \mathcal{B})$ plane of the bursting limit cycle for (a) $\gamma = 600$, (b) $\gamma = 800$ and (c) $\gamma = 1060$. Asterisks indicate the fixed point as discussed in the text. In (d) a detailed time trace of the bursting cycle is shown; plotted are $50|\mathcal{A}(1/2, T)|$, $\mathcal{B}(1/2, T)$ and $|\mathcal{A}(1/2, T)|$ at $\gamma = 800$.

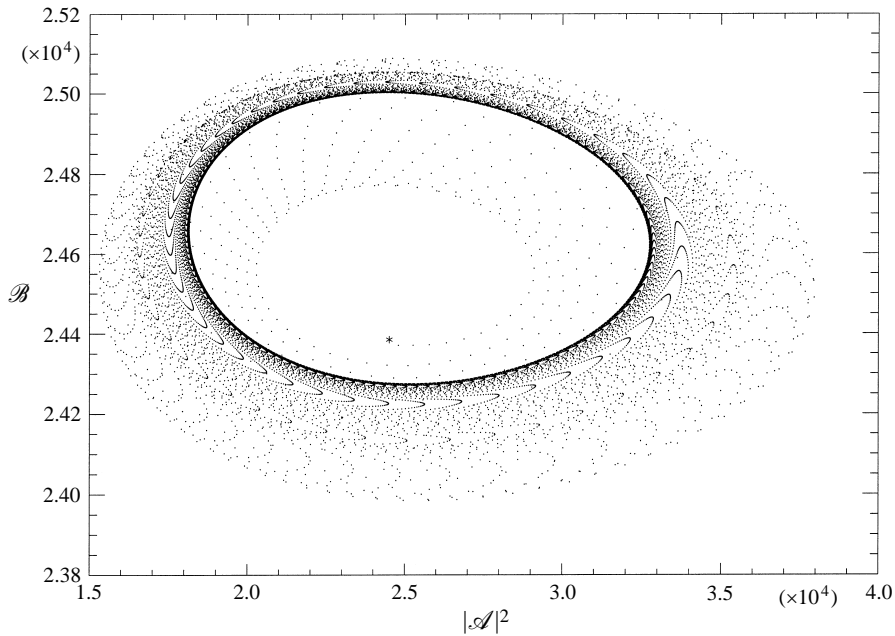


FIGURE 19. Phase portrait for $\gamma = 1500$ projected onto the $(|A|^2, B)$ plane. After a brief transient, the solution converges to a limit cycle which is not far from the fixed point. The latter is shown as an asterisk and serves as the initial condition for this time integration.

another limit cycle (in $|A|(1/2, T)|$) emerges. The bursting state also loses stability somewhere below $\gamma = 1500$. The result of this bifurcation is the state shown in figure 20. This solution still bursts in time, but, as is shown in figure 20, the bursts are irregular and no longer spatially symmetric. Here, vigorous convection sporadically appears at points all over the slot; also, there remains some tendency for the bursts to migrate vertically.

Finally, we point out that the bursting solution is typically the attractor that the system evolves to if the initial condition is one of low amplitude and γ is in the range 600–1000 (see figure 17). Hence, in practical situations, this is the state that one might find if one prepares the system in a quiescent state. In other words, the system might appear to undergo a hard transition and abruptly undergo sharp bursts as we introduce instability. This does not, however, signify subcritical linear instability.

9. Conclusion

We have conducted a study of linear stability for thermohaline convection in a tall thin slot, using a variety of boundary conditions. We observed that long-wave instability is a frequent occurrence, though it is not ubiquitous. Then, we derived long-wave equations for weakly nonlinear disturbances. The most general form of these equations is the *ABC* set given in §4.1.1; this contains all other variants of the problem, such as the *A* system of §4.1.3 and the Appendix, as special cases and includes a variety of other, more well known equations. Just as the complex Ginzburg–Landau equation governs the modulation of any finite- or short-wavelength patterns, so too the equations derived herein govern the evolution of general systems whose primary instability is of large length scale.

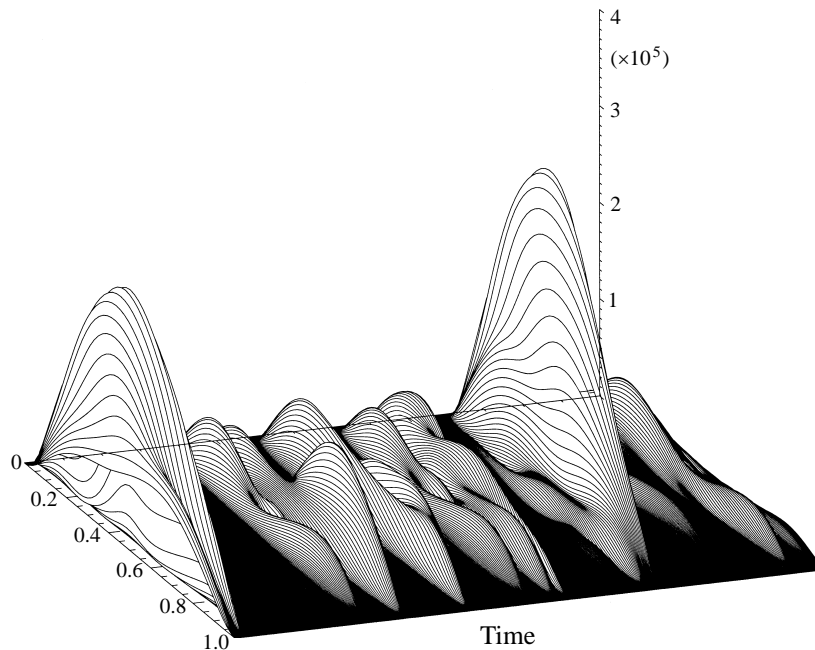


FIGURE 20. Space-time surface plot of $|\mathcal{A}|$ for $\gamma = 1500$. Amplitude is on the vertical axis and time increases to the right. The bursting solutions are both spatially asymmetric and temporally erratic.

Both the *ABC* system and the *A*-equation have stable equilibrium states just beyond the threshold of instability, and solutions that become complicated in both space and time, once the instability parameter becomes sufficiently large. There are multiple possible states for the system which suggests there may be pronounced hysteresis. Thus, the long-wave equations predict that doubly diffusive slot convection can take the form of a variety of different states from regular oscillatory patterns to irregular bursting events.

The *ABC* and *A* systems provide an interesting alternative to the usual complex Ginzburg-Landau style of weakly nonlinear theory which is often used in modelling spatio-temporal complexity. We emphasize that our study of the nonlinear dynamics has not been especially systematic. Our solutions suggest that the system possesses a wide range of behaviour, but we have only initiated the study of these systems, and hope we have provided some motivation for future work. For example, the various limits and dynamics of the equations offer exciting prospects: in certain limits we may open perturbation expansions that could help us understand the complicated dynamics, much as the dispersive limit of the complex Ginzburg-Landau equation has been utilized in the past.

In conclusion, we return to the fluid dynamics of the various problems that motivated this study. In any particular situation, the details of the original physical problem are most important, especially since we have seen that the boundary conditions can play a decisive role. This contrasts with the somewhat general approach we have taken here. None the less, one can attempt to draw some more general physical conclusions. One such important conclusion is that the convection will take the form of rolls that fill the slot, or become spatially irregular and burst locally. This prediction might seem a little difficult to reconcile with the observation that, in many situations, doubly diffusive instability leads to the formation of a thermohaline

staircase (Turner 1985); that is, persistent layers of overturning cells separated by diffusive interfaces. The reason why our system has not shown a tendency to form a staircase might be understandable in that layering is associated with strong instability, whereas we have been working in mildly supercritical conditions. Alternatively, in many situations, the boundary conditions are equivalent to fixed temperature, but no salt flux. This situation corresponds to an AC system, which is nonlinearly unstable; thus there may be a hard transition (one out of the applicability of our theory) that leads to layer formation.

Further experiments might help in understanding this apparent disagreement, but, as we noted at the outset, such experiments are quite difficult. The one which served as the motivation for this analysis (Biello 1996) was not executed very carefully and its failure should not be construed as a warning against such experiments, but rather as a challenge to clever experimentalists. In fact, there are other, more realistic experimental arrangements in which one could attain the necessary initial conditions to compare with our weakly nonlinear theory. For example, a slender, tall Hele-Shaw cell with a plate to one side would help to maintain the vertical temperature gradient and horizontal uniformity. Another might involve an apparatus exploiting a porous medium in which the substrate can itself help to maintain a horizontally uniform background temperature field. Finally, a thin cylindrical geometry (cf. Normand, 1984) could facilitate the constant, horizontally uniform, vertical temperature gradient which is the most difficult feature to achieve in all experiments.

This work began at the 1996 Geophysical Fluid Dynamics summer school at Woods Hole Oceanographic Institution; we thank Steve Meacham, the director, and all the participants for a productive summer. We thank W. R. Young and Y.-N. Young for helpful discussions. N.J.B. thanks the Green Foundation for support. J.A.B. acknowledges support from an NSF Graduate Fellowship.

Appendix. The fixed temperature and salinity system (the A -equation)

In this Appendix we describe some of the details of the A system. Rather than take the full equation of §4.2.2, for simplicity, we consider the simpler equation deriving from slaving the B - and C -modes according to §5.1. Hence we write the amplitude equation in the form

$$A_T = \gamma A + \eta A_{ZZ} + \Gamma A |A|_{ZZ}^2. \quad (\text{A } 1)$$

As for the ABC system we discuss certain limits of this equation, then describe some equilibrium solutions.

A.1. Some limits

There are two limits of the A -equation that are of special interest. These correspond to variational and conservative forms.

A.1.1. Real parameters

If γ , η and Γ are purely real, then the system has a Lyapunov functional

$$L[A] = \int_0^1 \left[\frac{1}{2} \Gamma (|A|_Z^2)^2 + \eta |A|_Z^2 - \gamma |A|^2 \right] dZ. \quad (\text{A } 2)$$

(From the equation of motion, one can show that this function must decay in time, and since the domain is finite, with side conditions, $A = 0$, it is bounded from below.)

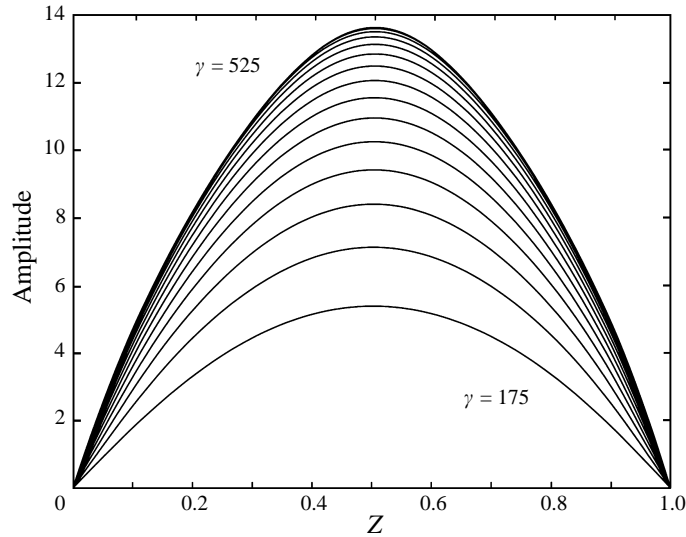


FIGURE 21. Equilibrium solutions for the A system. Shown are equilibria at $\gamma = 175$ to 525 in steps of 25 .

Thus the system asymptotically tends towards a state minimizing the integrand. This will be the lowest-order equilibrium solution, though in the relaxation process there may be prolonged meta-stable states just as in real Ginzburg–Landau theory (e.g. Balmforth 1995). Steady solutions for this special case are given by Normand (1984).

A.1.2. Imaginary parameters

If γ , η and Γ are all purely imaginary, then we may introduce a frequency factor and rescale the equation into the form

$$iA_T = A_{ZZ} + A|A|_{ZZ}^2; \quad (\text{A } 3)$$

that is, a long-wave analogue of the nonlinear Schrödinger equation. To find steady solutions, we introduce the solution $A = a(Z)e^{i\Omega T}$ and integrate to find the energy-like constant

$$E = \frac{1}{2}a_Z^2 + \frac{1}{4}(a^2)_Z^2 + \frac{1}{2}\Omega a^2. \quad (\text{A } 4)$$

Thence we may reduce the construction of the equilibrium solutions to a quadrature. However, simple phase plane arguments indicate that there are only ever periodic solutions in Z , and no solitary waves. One can further write the A system in a Hamiltonian form in this limit. However, this is not the place to continue such a discussion.

A.2. Equilibria and secondary stability

As for the ABC system we can again construct equilibrium solutions in both periodic and bounded domains. The periodic solutions, however, are rather special in the equation (A 1) since the nonlinear term always vanishes when $A \propto \exp iKZ$. In other words, the linear modes are exact nonlinear solutions of the equation, a somewhat unappealing state of affairs should they be unstable. We therefore consider only the bounded domain and construct solutions numerically.

Figure 21 shows the ($n = 1$) gravest equilibrium solution for various values of γ . In line with our earlier choice of parameters for case (ii), we take $\eta = (15, 4)$ and

$\Gamma = 0.06 + i$. As for the *ABC* system, secondary instability is commonplace. For the solutions shown in figure 21, this occurs for $\gamma \simeq 486.5$. Beyond this bifurcation, the solution relaxes to a higher-order ($n = 2$) equilibrium state, but more complicated dynamics can arise for different parameter settings. Also, when γ is sufficiently large, temporally complicated solutions appear. Hence the *A* system also appears to have a rich range of dynamical behaviour.

REFERENCES

- BALMFORTH, N. J. 1995 Solitary waves and homoclinic orbits. *Ann. Rev. Fluid Mech.* **27**, 335–373.
- BIELLO, J. A. 1996 Aspects of double diffusion in a thin slot. In *Double Diffusive Processes, 1996 Summer Study Program in Geophysical Fluid Dynamics*, WHOI Tech. Rep. WHOI-97-10.
- BREThERTON, C. S. & SPIEGEL, E. A. 1983 Intermittency through modulational instability. *Phys. Lett.* **96A**, 152–56.
- CASH, J. R. & SINGHAL, A. 1982 High order method for the numerical solution of two-point boundary value problems. *BIT* **22**, 184–188.
- CESSI, P., SPIEGEL, E. A. & YOUNG, W. R. 1990 Small-scale excitations in large systems. In *Nonlinear Evolution of Spatio-Temporal Structures in Dissipative Continuous Systems* (ed. F. H. Busse & L. Kramer). NATO ASI Series, vol. 255, pp. 231–236. Plenum.
- CESSI, P. & YOUNG, W. R. 1992 Fixed-flux convection in a tilted slot. *J. Fluid Mech.* **237**, 57–71.
- CHAPMAN, C. J. & PROCTOR, M. R. E. 1980 Nonlinear Rayleigh-Bénard convection between poorly conducting boundaries. *J. Fluid Mech.* **101**, 759–782.
- CHATÉ, H. 1994 Spatiotemporal intermittency regimes of the one-dimensional complex Ginzburg-Landau equation. *Nonlinearity* **7**, 185–204.
- CHEN, C. F., BRIGGS, D. G. & WHIRTZ, R. A. 1971 Stability of thermal convection in a salinity gradient due to lateral heating. *Intl J. Heat Mass Transfer* **14**, 57–65.
- CHEN, C. F. & TURNER, J. S. 1980 Crystallization in a double-diffusive system. *J. Geophys. Res.* **85**, 2573.
- CHILDRESS, S. & SPIEGEL, E. A. 1981 A prospectus for a theory of variable variability. In *Variations of the Solar Constant* (ed. S. Sofia). NASA Conf. Pub. 2191, p. 273.
- HUPPERT, H. E. & LINDEN, P. F. 1979 On heating a stable salinity gradient from below. *J. Fluid Mech.* **96**, 431–464.
- JANIAUD, B., PUMIR, A., BENSIMON, D., CROQUETTE, V., RICHTER, H. & KRAMER, L. 1992 The Eckhaus instability for travelling waves. *Physica D* **55**, 269–286.
- LAPWOOD, E. R. 1948 Convection of fluid in a porous medium. *Proc. Camb. Phil. Soc.* **44**, 508–521.
- LINZ, S. 1990 Naturally driven dispersion in tilted porous layers. In *Proc. Woods Hole Oceanographic Inst. Summer Study Program in Geophysical Fluid Dynamics* WHOI 91-03.
- MURRAY, B. T. & CHEN, C. F. 1989 Doubly diffusive convection in a porous medium. *J. Fluid Mech.* **201**, 147–166.
- NORMAND, C. 1984 Nonlinear convection in high vertical channels. *J. Fluid Mech.* **143**, 223–242.
- PEARLSTEIN, A. J. 1981 Effect of rotation on the stability of a doubly diffusive fluid layer. *J. Fluid Mech.* **103**, 389–412.
- PISMEN, L. M. 1988 Selection of long-wave oscillatory convective patterns. *Phys. Rev. A* **38**, 2564–2572.
- POYET, J.-P. 1981 Time-dependent convection. PhD thesis, Columbia University.
- PROCTOR, M. R. E. & HOLYER, J. Y. 1986 Planform selection in salt fingers. *J. Fluid Mech.* **168**, 241–253.
- SAARLOOS, W. VAN & HOHENBERG, P. C. 1992 Fronts, pulses, sources and sinks in generalized complex Ginzburg-Landau equations. *Physica D* **56**, 303–367.
- SPRUIT, H. C. 1992 The rate of mixing in semiconvective zones. *Astron. Astrophys.* **253**, 131–138.
- TURNER, J. S. 1985 Multicomponent convection. *Ann. Rev. Fluid Mech.* **17**, 11–44.
- VERONIS, G. 1968 Effect of a stabilizing gradient of solute on thermal convection. *J. Fluid Mech.* **34**, 315–336.